

Genetic Screens Identify a Context-Specific PI3K/p27^{Kip1} Node Driving Extrahepatic Biliary Cancer



Chiara Falcomatà^{1,2,3}, Stefanie Bärthel^{1,2,3}, Angelika Ulrich^{1,2}, Sandra Diersch⁴, Christian Veltkamp^{1,2,3}, Lena Rad^{1,2,3}, Fabio Boniolo^{1,2,3}, Myriam Solar⁵, Katja Steiger^{6,7}, Barbara Seidler^{1,2,3,4}, Magdalena Zukowska^{1,2,3,4}, Joanna Madej^{1,2,3}, Mingsong Wang^{1,2,3,4}, Rupert Öllinger^{3,7,8}, Roman Maresch^{3,7,8}, Maxim Barenboim^{7,8,9}, Stefan Eser^{1,2,4}, Markus Tschurtschenthaler^{1,2,3}, Ariane Mehrabi¹⁰, Stephanie Roessler¹¹, Benjamin Goeppert¹¹, Alexander Kind¹², Angelika Schnieke¹², Maria S. Robles¹³, Allan Bradley¹⁴, Roland M. Schmid⁴, Marc Schmidt-Supprian^{3,7,15}, Maximilian Reichert^{4,7,16}, Wilko Weichert^{6,7}, Owen J. Sansom^{5,17}, Jennifer P. Morton^{5,17}, Roland Rad^{3,7,8}, Günter Schneider^{4,7,18}, and Dieter Saur^{1,2,3,4}

ABSTRACT

Biliary tract cancer ranks among the most lethal human malignancies, representing an unmet clinical need. Its abysmal prognosis is tied to an increasing incidence and a fundamental lack of mechanistic knowledge regarding the molecular basis of the disease. Here, we show that the Pdx1-positive extrahepatic biliary epithelium is highly susceptible toward transformation by activated PIK3CA^{H1047R} but refractory to oncogenic Kras^{G12D}. Using genome-wide transposon screens and genetic loss-of-function experiments, we discover context-dependent genetic interactions that drive extrahepatic cholangiocarcinoma (ECC) and show that PI3K signaling output strength and repression of the tumor suppressor p27^{Kip1} are critical context-specific determinants of tumor formation. This contrasts with the pancreas, where oncogenic Kras in concert with p53 loss is a key cancer driver. Notably, inactivation of p27^{Kip1} permits Kras^{G12D}-driven ECC development. These studies provide a mechanistic link between PI3K signaling, tissue-specific tumor suppressor barriers, and ECC pathogenesis, and present a novel genetic model of autochthonous ECC and genes driving this highly lethal tumor subtype.

SIGNIFICANCE: We used the first genetically engineered mouse model for extrahepatic bile duct carcinoma to identify cancer genes by genome-wide transposon-based mutagenesis screening. Thereby, we show that PI3K signaling output strength and p27^{Kip1} function are critical determinants for context-specific ECC formation.

¹Division of Translational Cancer Research, German Cancer Research Center (DKFZ) and German Cancer Consortium (DKTK), Heidelberg, Germany. ²Chair of Translational Cancer Research and Institute for Experimental Cancer Therapy, Klinikum rechts der Isar, School of Medicine, Technische Universität München, Munich, Germany. ³Center for Translational Cancer Research (TranslaTUM), School of Medicine, Technical University of Munich, Munich, Germany. ⁴Department of Internal Medicine II, Klinikum rechts der Isar, Technische Universität München, Munich, Germany. ⁵Cancer Research UK Beatson Institute, Glasgow, United Kingdom. ⁶Institute of Pathology, Klinikum rechts der Isar, Technische Universität München, München, Germany. ⁷German Cancer Consortium (DKTK), Heidelberg, Germany. ⁸Institute of Molecular Oncology and Functional Genomics, School of Medicine, Technische Universität München, Munich, Germany. ⁹Department of Pediatrics and Children's Cancer Research

Center, Klinikum rechts der Isar, Technische Universität München, School of Medicine, Munich, Germany. ¹⁰Department of Surgery, Universität Heidelberg, Heidelberg, Germany. ¹¹Institute of Pathology, Universität Heidelberg, Heidelberg, Germany. ¹²Livestock Biotechnology, Technische Universität München, Freising, Germany. ¹³Institute of Medical Psychology, Faculty of Medicine, LMU Munich, Munich, Germany. ¹⁴Wellcome Trust Sanger Institute, Genome Campus, Hinxton-Cambridge, United Kingdom. ¹⁵Institute of Experimental Hematology, School of Medicine, Technische Universität München, Munich, Germany. ¹⁶Center for Protein Assemblies (CPA), Technische Universität München, Garching, Germany. ¹⁷Institute of Cancer Sciences, University of Glasgow, Glasgow, United Kingdom. ¹⁸Department of General, Visceral and Pediatric Surgery, University Medical Center Göttingen, Göttingen, Germany.



INTRODUCTION

Adenocarcinomas of the bile duct express markers of cholangiocyte differentiation and are therefore termed cholangiocarcinomas (CC). They are classified into three subtypes, depending on their distinct anatomical location within the biliary tree: intrahepatic CC (ICC; comprising 10%–20% of all cases), and extrahepatic CC (ECC) with perihilar (PCC; 50%–60%) and distal (DCC; 20%–30%) location (1). This group of cancers is heterogeneous, and the anatomical subtypes differ not only in their anatomical site, but also in their epidemiology, pathogenesis, and genetic and clinical characteristics.

C. Falcomatà, S. Bärthel, and A. Ulrich contributed equally to this work and share first authorship.

R. Rad, G. Schneider, D. Saur contributed equally to this work and share senior authorship.

Corresponding Authors: Dieter Saur, Chair of Translational Cancer Research, Technical University of Munich, Ismaningerstr. 22, Munich, 81675, Germany. Phone: 49-89-4140-5255; Fax: 49-89-4140-7289; E-mail: dieter.saur@tum.de; and Günter Schneider, guenter.schneider@tum.de

This is reflected in different treatment options and therapeutic responses (1–3). CC develops from cholangiocytes or their progenitor cells lining the biliary tract, which arise from two distinct developmental origins. The intrahepatic biliary tree derives from liver progenitor cells, called hepatoblasts, which give rise to hepatocytes and intrahepatic cholangiocytes (4). The extrahepatic part of the biliary tree develops before the intrahepatic tract, and both systems merge at the level of the hepatic duct during embryonic development. Cholangiocytes lining the extrahepatic bile ducts share a common origin with the ventral pancreas, but not the liver. They derive from

Cancer Discov 2021;11:3158–77

doi: 10.1158/2159-8290.CD-21-0209

This open access article is distributed under the Creative Commons Attribution-NonCommercial-NoDerivatives 4.0 International (CC BY-NC-ND 4.0) license.

©2021 The Authors; Published by the American Association for Cancer Research

Pdx1-positive progenitor cells from the caudal part of the ventral foregut endoderm (4, 5).

The incidence of biliary tract cancer (BTC), which is highest in South/East Asia and South America, is increasing worldwide (1, 6). In the Western world, BTC accounts for 3% of all gastrointestinal tumors, with ECC being the most common type of BTC (1, 2). Despite modern multimodal treatment regimes, mortality rates of bile duct cancer have remained stubbornly unchanged for the last three decades, with approximately 10% of patients surviving 5 years (1–3, 7). This contrasts with other solid tumor entities such as colorectal cancers, where death rates have decreased more than 40% over the past 20 years (8). Surgical resection is the procedure of choice. However, early symptoms are unspecific and, by the time of diagnosis, most tumors are not surgically resectable. Consequently, there is an urgent need to identify and validate actionable cancer drivers as novel therapeutic targets.

Comprehensive molecular tumor profiling has greatly improved our understanding of the processes underlying tumorigenesis in the biliary tract (1, 3, 9–12). These studies revealed a subtype-associated prevalence of genomic alterations, methylation pattern, and gene-expression profiles in line with the observed clinicopathologic differences between ICC and ECC (2, 3, 11, 13). However, we are still far from understanding the nature of the described genetic alterations, their functional relevance, their downstream effectors, and their role in oncogenic networks. Specifically, mechanistic knowledge concerning true cancer drivers remains extremely poor for ECC, which is in part due to a lack of genetically defined animal models that accurately mimic this tumor subtype. Improving the survival of patients with ECC will therefore depend on unbiased functional systematic approaches in relevant model systems to identify the genes and pathways that drive the disease.

To this end, we generated a Cre/loxP-based genetically engineered mouse model (GEMM) of bile duct cancer with consequent extrahepatic localization and performed a forward genetic screen using the conditional *piggyBac* transposon mutagenesis system (14, 15). Analysis of recurrent transposon insertion sites identified numerous cancer genes and pathways, including known and new ECC-related genes, providing a unique resource for novel potential therapeutic targets. We used loss-of-function experiments in GEMMs to validate selected therapeutically tractable pathways and uncovered unexpected context-specific oncogenic networks, genetic dependencies, and tumor-suppressive functions in ECC development.

RESULTS

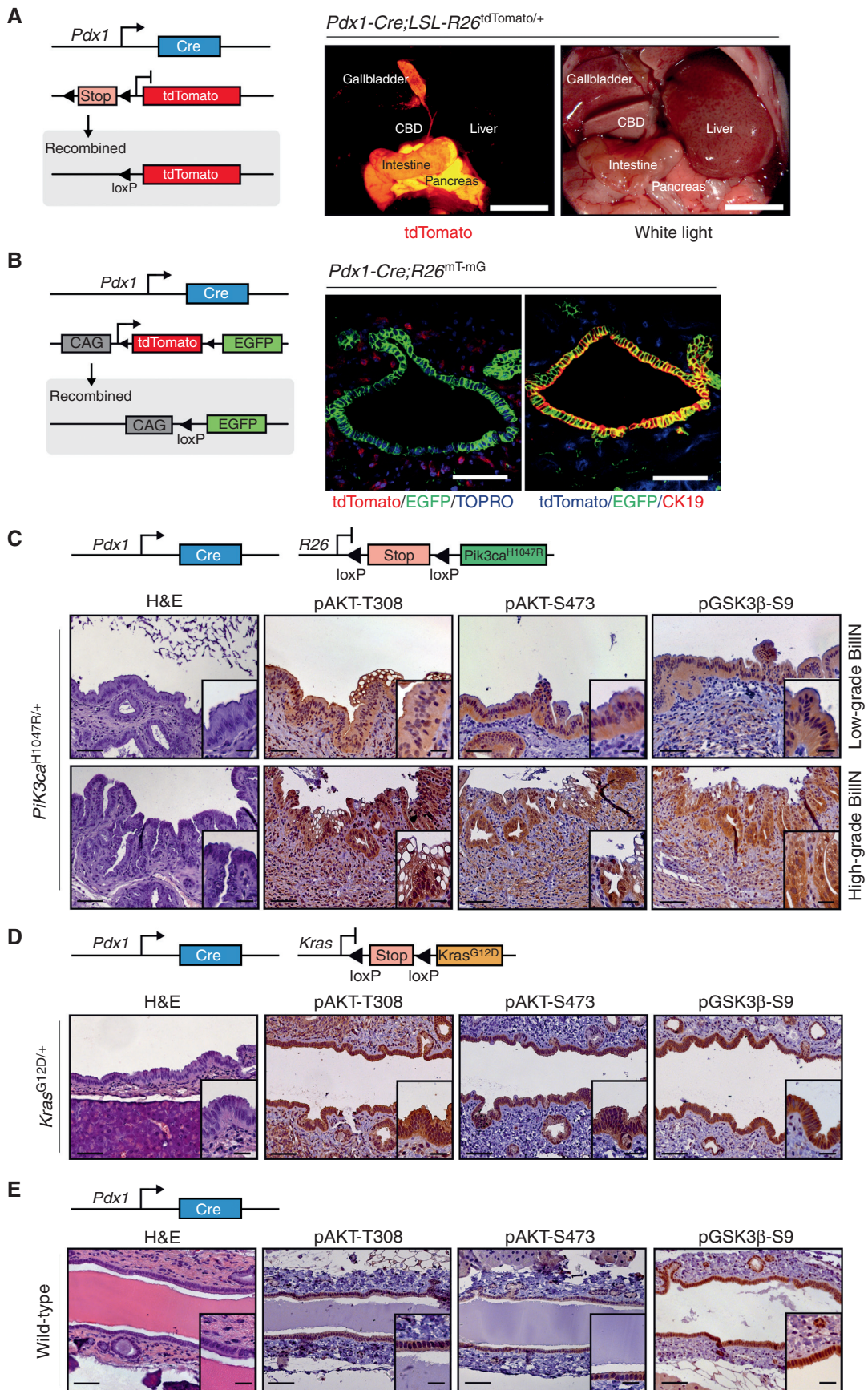
Pdx1-Cre Mediated Genetic Manipulation of the Extrahepatic Biliary Epithelium

To target the extrahepatic biliary epithelium, we used transgenic mice expressing Cre recombinase under the control of the murine *Pdx1* promoter (ref. 16; *Pdx1*-Cre; Fig. 1A and B; Supplementary Fig. S1A). We evaluated the patterns of *Pdx1*-Cre transgene expression using two different Cre activatable reporter alleles. A lox-stop-lox (LSL) silenced fluorescent tdTomato reporter line (*LSL-R26^{tdTomato/+}*; Fig. 1A; ref. 17) and a switchable floxed double-color fluorescent tdTomato-EGFP Cre reporter allele (*R26^{mT-mG}*) that replaces the expression of tdTomato with EGFP after Cre-mediated recombination (Fig. 1B; ref. 18). Macroscopic fluorescence stereomicroscopy of *Pdx1*-Cre;*LSL-R26^{tdTomato/+}* mice revealed Cre-mediated recombination of the extrahepatic biliary tree, the pancreas, and duodenum *in vivo*, as evidenced by tdTomato expression (Fig. 1A). Using genetic *Pdx1*-Cre;*R26^{mT-mG}* reporter animals, we confirmed Cre-mediated recombination specifically in the extrahepatic bile duct histologically, as shown by expression of membrane-tagged EGFP in CK19-positive biliary epithelial cells and peribiliary glands (Fig. 1B). In contrast, stromal cells remained unrecombined and expressed membrane-tagged tdTomato (Fig. 1B). No recombination was observed by fluorescence microscopy and genotyping PCR in liver, lung, kidney, heart, colon, brain, and spleen (Fig. 1; Supplementary Fig. S1A).

Activation of Oncogenic *Pik3ca^{H1047R}* but Not *Kras^{G12D}* Induces Premalignant Biliary Intraepithelial Neoplasia

Molecular profiling of human BTC revealed a large set of putative cancer drivers that are enriched for the RAS-RAF-MEK-ERK, PI3K-AKT-mTOR, TGF β , and growth factor receptor signaling pathways, as well as epigenetic regulators and DNA damage response genes (1, 3, 10, 12, 13, 19–23). However, the functional consequences of these putative driver alterations and their relevance for ECC development have not been investigated *in vivo*. To test whether constitutive activation of oncogenic *Kras* or *Pik3ca*, which regulates two of the most frequently altered oncogenic pathways in BTC (3), is capable of transforming the extrahepatic biliary epithelium *in vivo*, we used the *Pdx1*-Cre model. We used an LSL-silenced oncogenic *Pik3ca^{H1047R}* allele as a knock-in at the *Rosa26* locus (*LSL-Pik3ca^{H1047R/+}* line; Fig. 1C; Supplementary Graphical Abstract and Supplementary Fig. S1A; ref. 24) to explore the mechanistic role of the PI3K-AKT-mTOR signaling pathway

Figure 1. Constitutive activation of the PI3K signaling pathway induces premalignant biliary intraepithelial neoplasia (BillN). **A**, Left: genetic strategy and recombination scheme to analyze the patterns of *Pdx1*-Cre transgene expression using a conditional tdTomato reporter allele (*LSL-R26^{tdTomato/+}*). Right: macroscopic fluorescence and white-light images of the *Pdx1*-Cre;*LSL-R26^{tdTomato/+}* reporter mouse. Visualization of tdTomato reveals reporter gene expression (red) in the pancreas, duodenum, gallbladder, and common bile duct (CBD). Scale bars, 1 cm. **B**, Left: genetic strategy and recombination scheme to analyze the patterns of *Pdx1*-Cre transgene expression using a switchable floxed double-color fluorescent tdTomato-EGFP Cre reporter line (*R26^{mT-mG}*). Right panel, left image: representative confocal microscopic image of tdTomato (red color, non-Cre-recombined cells) and Cre-induced EGFP (green color) expression in the common bile duct. Note: Cre-mediated EGFP expression in the biliary epithelium and peribiliary glands, but not stromal cells. Nuclei were counterstained with TOPRO-3 (blue). Right image: representative immunofluorescence staining of CK19 (red color) of *Pdx1*-Cre;*R26^{mT-mG/+}* animal. Note: Blue color shows expression of tdTomato in unrecombined cells. Green color labels Cre-recombined cells that express EGFP. Colocalization of CK19 immunofluorescence staining (red) and EGFP expression (green) results in yellow color. Scale bars, 50 μ m. **C–E**, Genetic strategy used to express oncogenic *Pik3ca^{H1047R}* (**C**), *Kras^{G12D}* (**D**), or only Cre as control (**E**) in the common bile duct (top). Hematoxylin and eosin (H&E) staining and IHC analysis of PI3K/AKT pathway activation in the biliary epithelium of the common bile duct and different grades of dysplasia in BillN (bottom). Scale bars, 50 μ m for micrographs and 20 μ m for insets.



in ECC development. This mouse line carries a histidine (H) to arginine (R) mutation at codon 1047 (H1047R) within the highly conserved kinase domain of *Pik3ca*, resulting in increased catalytic activity and enhanced PI3K downstream signaling (24, 25). To achieve conditional activation of oncogenic *Kras* in the *Pdx1-Cre* lineage, we used a latent *Kras*^{G12D} allele as a knock-in at the endogenous *Kras* locus (*LSL-Kras*^{G12D/+} line; Fig. 1D; Supplementary Fig. S1A and Supplementary Graphical Abstract; ref. 16). This mouse line carries a glycine (G) to aspartic acid (D) mutation at codon 12 (G12D) of *Kras*, which is refractory to GTPase-activating protein (GAP)-induced GTP hydrolysis, favoring an active state (26). Expression of mutationally activated *Pik3ca*^{H1047R} in *Pdx1-Cre;LSL-Pik3ca*^{H1047R/+} mice revealed no overt phenotype after birth. However, adult animals developed an enlarged extrahepatic bile duct and biliary intraepithelial neoplasia (BillIN; Fig. 1C; Supplementary Fig. S1B), a precursor lesion of ECC (27) with complete penetrance. The grade of BillIN lesions increased over time; from low-grade BillINs in young animals to high-grade lesions in 9-month-old animals. In contrast to the *Pik3ca*^{H1047R} model, the extrahepatic bile duct was refractory toward neoplastic transformation by oncogenic *Kras*^{G12D} (Fig. 1D; Supplementary Fig. S1B). Instead, *Kras*^{G12D} expression in the *Pdx1-Cre* lineage induced only acinar–ductal metaplasia (ADM) and pancreatic intraepithelial neoplasia (PanIN), a precursor to invasive pancreatic ductal adenocarcinoma (PDAC). We observed similar lesions in a previous study in the pancreas after selective activation of *Pik3ca*^{H1047R} in pancreatic precursor cells using a *Ptf1a*^{Cre} line (24).

To compare *Pik3ca* expression levels between mutant and wild-type tissue and assess the activation status of the PI3K signaling pathway in *Pik3ca*^{H1047R}- and *Kras*^{G12D}-mutant mice, we analyzed the common bile duct by IHC (Fig. 1C–E; Supplementary Fig. S1C). As expected, *Pik3ca* expression levels were moderately increased in the bile duct of *Pik3ca*^{H1047R}-mutant animals in comparison with wild-type mice (Supplementary Fig. S1C). In line with this, we observed activation of key downstream effectors of PI3K signaling, such as pAKT-T308, pAKT-S473, and pGSK3β-S9 (Fig. 1C). Interestingly, PI3K signaling is also activated in the extrahepatic bile duct of *Kras*^{G12D}-mutant and wild-type mice, albeit to a lesser extent than in the wild-type (Fig. 1D and E). This indicates that signaling thresholds and tumor suppressor barriers might be important determinants of oncogenic transformation.

Pdx1-Cre-mediated activation of oncogenic *Pik3ca*^{H1047R} or *Kras*^{G12D} in the pancreas resulted in very similar patterns of ADM and PanIN induction (Supplementary Fig. S2A and S2B). Surrogate markers of PI3K signaling were almost identical in *Pik3ca*^{H1047R}- and *Kras*^{G12D}-driven tumors, as shown by phospho-specific pAKT-T308, pAKT-S473, and pGSK3β-S9 stainings, indicating an important role of this pathway for PDAC formation (Supplementary Fig. S2B and S2C). Previous studies validated its essential role for PanIN and PDAC development by genetic loss-of-function experiments in *Kras*^{G12D}-driven GEMMs (24, 28).

To assess the signaling output of the canonical MAPK pathway, we analyzed ERK 1/2 activation using a phosphorylation-specific antibody. MAPK pathway signaling was decreased in the bile duct of the *Pik3ca*^{H1047R} model compared with wild-type animals. In the pancreas, we observed strong

ERK 1/2 activation in *Kras*^{G12D}-driven PanINs and PDAC, whereas *Pik3ca*^{H1047R}-induced tumors showed lower phosphorylation levels (Supplementary Fig. S2B–S2D).

Taken together, our data demonstrate that activation of oncogenic *Pik3ca*^{H1047R} in the extrahepatic bile duct models the full spectrum of human BillIN precursor lesion progression. In addition, they uncover fundamental different context-specific oncogenic vulnerabilities of the extrahepatic bile duct and the pancreas, although both organs originate from the same Pdx1-positive precursor cell lineage.

Expression of Mutant *Pik3ca*^{H1047R} Induces Invasive ECC

To test whether *Pik3ca*^{H1047R} is capable of inducing ECC, we aged *Pdx1-Cre;LSL-Pik3ca*^{H1047R/+} mice. Within 800 days, 90% of the *Pik3ca*^{H1047R}-mutant animals in the tumor watch cohort developed extrahepatic bile duct cancer (Fig. 2A–D; Supplementary Graphical Abstract) displaying strong PI3K/AKT pathway activation, as demonstrated by key downstream surrogates of PI3K signaling: AKT-T308/S473 and GSK3β-S9 phosphorylation (Fig. 2B). ECCs recapitulated the full spectrum of the human disease, ranging from well-differentiated, stroma-rich ductal adenocarcinomas to more undifferentiated tumors (Fig. 2B; Supplementary Fig. S2; refs. 27, 29). Notably, at the time of necropsy, all animals developing ECC displayed cholestasis with bile duct obstruction and jaundice. This caused termination of the experiment as humane endpoint. Thus, the new *Pdx1-Cre;LSL-Pik3ca*^{H1047R/+} model faithfully mimics human ECC; from precursor lesion formation and progression to full-blown bile duct-obstructing invasive cancers, with a characteristic strong desmoplastic stromal reaction (27, 29).

Comparison of tumor formation of *Pik3ca*^{H1047R}- and *Kras*^{G12D}-mutant animals revealed striking differences. Although survival times were nearly identical, *Kras*^{G12D}-mutant mice developed exclusively invasive tumors of the pancreas, recapitulating PDAC, but not BTC (Fig. 2C and D; Supplementary Fig. S3A and Supplementary Graphical Abstract). We never observed high-grade BillIN lesions or invasive ECC in *Kras*^{G12D}-mutant animals aged up to 800 days. This unexpected resistance of the extrahepatic biliary epithelium against oncogenic transformation by *Kras*^{G12D} contrasts with other tissue types, such as the lung or the intrahepatic biliary tract, which are highly susceptible to *Kras*^{G12D}-induced tumorigenesis (24, 30, 31).

To assess tumor development in other *Pdx1-Cre* recombined organs in *Pik3ca*^{H1047R}-mutant mice (see Fig. 1A; Supplementary Fig. S1A), we performed a comprehensive macroscopic and microscopic histopathologic analysis and observed PDAC development in 60%, hyperplasia of the duodenal mucosa in 100%, and duodenal adenoma formation in 10% of the investigated double-transgenic animals (Fig. 2D; Supplementary Fig. S3A–S3C). Histopathologic analyses revealed that *Pik3ca*^{H1047R}-induced tumors were indistinguishable from *Kras*^{G12D}-driven PDAC and showed the full spectrum of the disease, including ADM and PanIN lesions (Fig. 2; Supplementary Fig. S3A).

Together, these data support the notion that PI3K signaling is an important functional driver of ECC development and suggest that distinct context-specific tumor suppressor

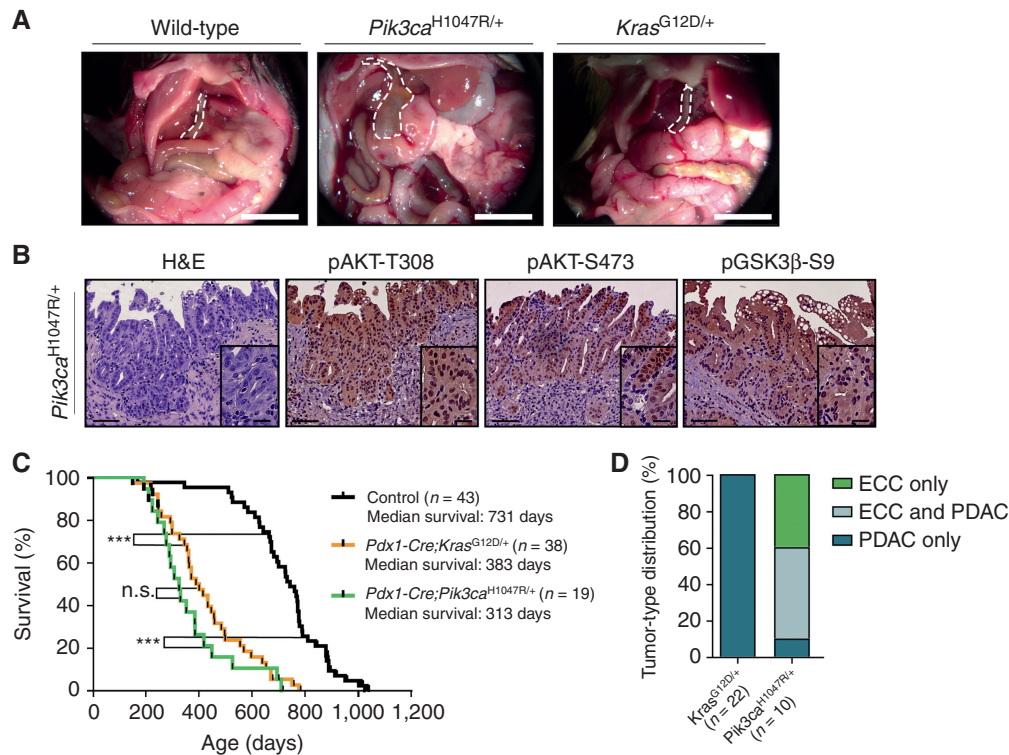


Figure 2. Expression of oncogenic *Pik3ca*^{H1047R} but not *Kras*^{G12D} induces ECC. **A**, Representative *in situ* images of 12-month-old wild-type (control), *Pdx1-Cre;LSL-Pik3ca*^{H1047R/+}, and *Pdx1-Cre;LSL-Kras*^{G12D/+} mice. The common bile duct is outlined by a white dashed line. Scale bars, 1 cm. **B**, Representative hematoxylin and eosin (H&E) stainings and IHC analyses of PI3K/AKT pathway activation in the common bile duct of aged *Pdx1-Cre;LSL-Pik3ca*^{H1047R/+} mice with invasive ECC. Scale bars, 50 μ m for micrographs and 20 μ m for insets. **C**, Kaplan-Meier survival curves of the indicated genotypes (n.s., not significant; ***, $P < 0.001$, log-rank test). **D**, Tumor-type distribution in percentage according to histologic analysis of the extrahepatic bile duct and the pancreas from *Pdx1-Cre;LSL-Kras*^{G12D/+} and *Pdx1-Cre;LSL-Pik3ca*^{H1047R/+} mice.

barriers and/or signaling thresholds are operative in the pancreas and the extrahepatic bile duct. This is remarkable due to the shared developmental origin of the pancreas and the extrahepatic bile duct and, therefore, a common cell of origin of both tissue types.

Oncogenic PI3K Signaling Activates a Senescence Program in the Extrahepatic Bile Duct That Is Independent of the p53 Pathway

We next analyzed tissue-specific tumor-suppressive mechanisms in the *Pik3ca*^{H1047R} model. Expression of oncogenic *Pik3ca*^{H1047R} induced a senescence program in the extrahepatic biliary epithelium, similar to the activation of oncogenic *Kras*^{G12D} in the pancreas (Fig. 3A; Supplementary Graphical Abstract; ref. 32). Low-grade BilIN lesions but not wild-type epithelium stained positive for senescence-associated β -galactosidase (SA- β -Gal), which has been shown to be a reliable oncogene-induced senescence (OIS) biomarker (Fig. 3A; ref. 33). OIS can be induced by the tumor suppressor p53 and its target gene p21^{Cip1}. Interestingly, and in contrast to *Pik3ca*^{H1047R}- and *Kras*^{G12D}-induced ADM and PanINs in the pancreas, BilIN lesions lack activation of the canonical p53–p21^{Cip1} senescence pathway (Fig. 3A) and display significantly reduced levels of apoptotic cell death (Fig. 3B and C). Previously, it has been shown that OIS and apoptotic cell death are triggered by the p53 network in the pancreas (32,

34). The absence of p53 induction and the significantly lower levels of apoptosis in the extrahepatic bile duct versus the pancreas upon *Pik3ca*^{H1047R} activation indicate fundamental context-dependent differences in the genetic networks and tumor suppressor barriers that prevent tumor formation in both organs (Supplementary Graphical Abstract).

To elucidate the role of the p53 pathway in ECC and PDAC formation functionally, we inactivated *Trp53* genetically using floxed *Trp53* mice (35). Strikingly, at the humane endpoint, we observed a significantly reduced survival of *Trp53*-deleted animals and a shift of the tumor spectrum from ECC to PDAC in the *Pik3ca*^{H1047R} model, whereas *Kras*^{G12D};*Trp53*^{f/+} animals again developed PDAC only (Fig. 3D–G; Supplementary Graphical Abstract). To investigate the timing and order of BilIN/PanIN and ECC/PDAC formation in this model, we analyzed *Pik3ca*^{H1047R};*Trp53*^{f/+} mice without clinical signs of cancer development at two selected early time points. This revealed widespread occurrence of low- and high-grade BilIN lesions along the extrahepatic bile duct already in 1.5-month-old animals, whereas only a few ADMs and even less low-grade PanIN lesions were present in the pancreas (Supplementary Fig. S4A). Nevertheless, most *Trp53*-deleted animals at the endpoint displayed PDAC and BilINs, but not invasive ECC (Fig. 3E). Only one mouse at an age of 3 months developed invasive PDAC and ECC in parallel in the same animal (Supplementary Fig. S4B). This indicates that BilIN

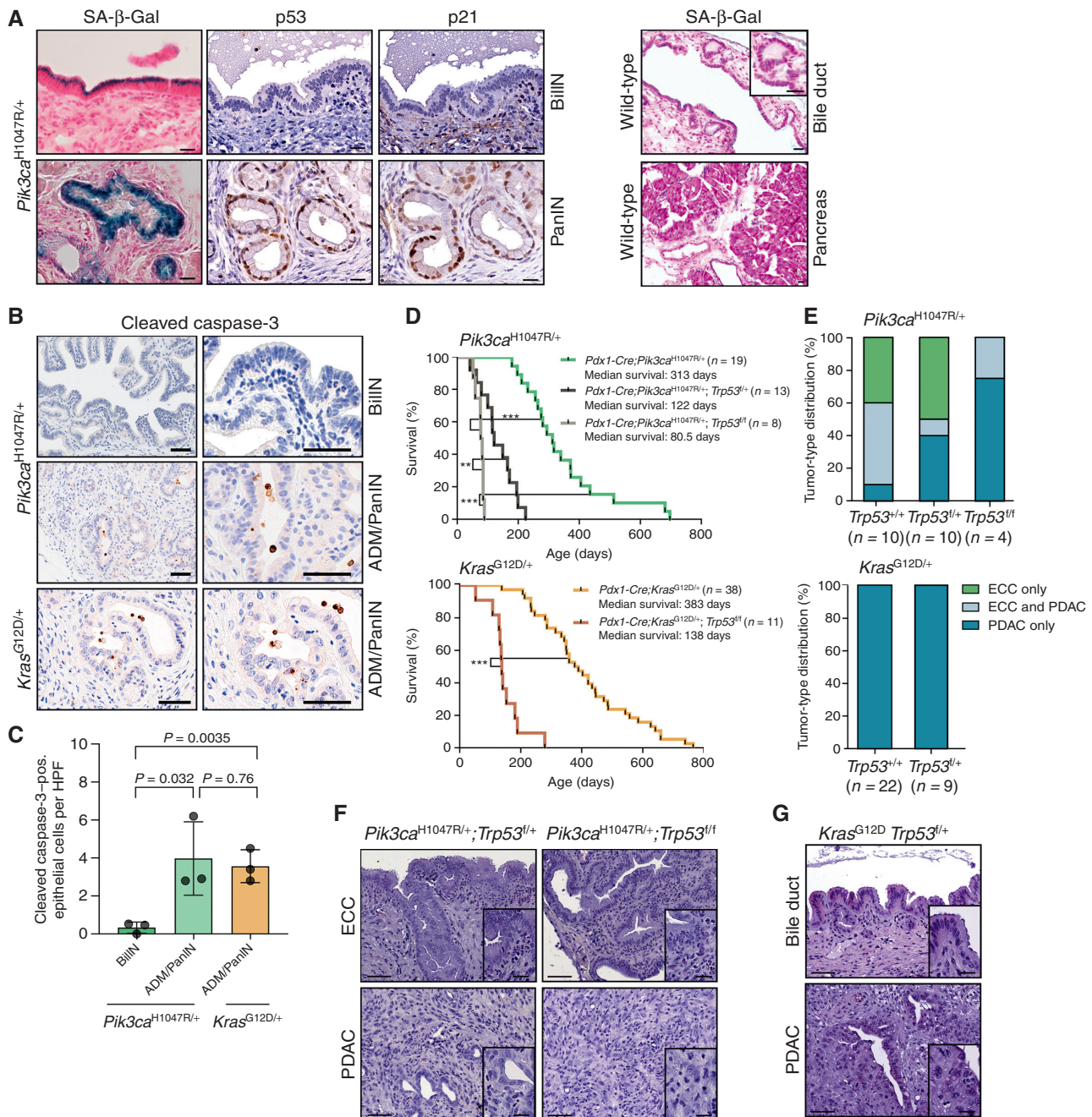


Figure 3. Oncogenic PI3K signaling induces senescence in the extrahepatic bile duct that is independent of the Trp53 pathway. **A**, Left, representative SA-β-Gal staining, and p53 and p21 IHC of BiliN (top) and PanIN (bottom) lesions of a $Pdx1-Cre;Pik3ca^{H1047R/+}$ mouse. Right, representative SA-β-Gal staining of wild-type extrahepatic bile duct and pancreas. Scale bars, 20 μm. **B**, Representative IHC cleaved caspase-3 staining of BiliN and ADM/PanIN of a $Pdx1-Cre;LSL-Pik3ca^{H1047R/+}$ mouse and an ADM/PanIN of $Pdx1-Cre;LSL-Kras^{G12D/+}$ mouse. Scale bars, 50 μm. **C**, Quantification of cleaved caspase-3-positive epithelial cells in BiliN and ADM/PanIN lesions of the indicated genotypes. Each dot represents one animal (mean ± SD; P values are indicated, two-tailed Student t test). HPF, high-power field; pos., positive. **D**, Kaplan-Meier survival curves of the indicated genotypes (**, $P < 0.01$; ***, $P < 0.001$, log-rank test). **E**, Top: tumor-type distribution according to histologic analysis of the extrahepatic bile duct and pancreas of $Pdx1-Cre;LSL-Pik3ca^{H1047R/+};p53^{fl/fl}$, and $Pdx1-Cre;LSL-Pik3ca^{H1047R/+};p53^{fl/fl}$ mice. Note: Reduced ECC fraction in mice with the $Pdx1-Cre;Pik3ca^{H1047R/+};p53^{fl/fl}$ genotype ($P = 0.02$, Fisher exact test). Bottom: tumor-type distribution according to histologic analysis of the extrahepatic bile duct and pancreas of $Pdx1-Cre;LSL-Kras^{G12D/+}$ and $Pdx1-Cre;LSL-Kras^{G12D/+};p53^{fl/fl}$ mice. **F**, Representative hematoxylin and eosin (H&E) staining of ECC and PDAC of $Pdx1-Cre;LSL-Pik3ca^{H1047R/+};p53^{fl/fl}$ and $Pdx1-Cre;LSL-Pik3ca^{H1047R/+};p53^{fl/fl}$ mice. **G**, Representative H&E staining of the common bile duct and PDAC of a $Pdx1-Cre;LSL-Kras^{G12D/+};p53^{fl/fl}$ mouse. Scale bars, 50 μm for micrographs and 20 μm for insets. The $Pdx1-Cre;Pik3ca^{H1047R/+}$ and $Pdx1-Cre;LSL-Kras^{G12D/+}$ cohorts shown in **D** and **E** are the same as those shown in Fig. 2C and D.

development may precede PanINs; however, deletion of *Trp53* accelerates progression of low-grade PanIN precursor lesions to invasive pancreatic cancer, leading to a substantial shift in the tumor spectrum toward PDAC. These findings support the view of tissue-specific tumor-suppressive functions of p53 being a pivotal tumor barrier in the pancreas (Supplementary Graphical Abstract).

Identification of Cancer Genes in the Extrahepatic Biliary Tract by a *PiggyBac* Transposon Mutagenesis Screen

To study cooperating genetic events in extrahepatic bile duct cancer, we used a previously developed conditional *piggyBac* transposon-based somatic insertional mutagenesis system in mice with activated *Pik3ca*^{H1047R} (14). To this end, we crossed an *LSL*-silenced *piggyBac* transposase allele (*LSL-R26^{PB}*) with ATP1-S2 mice, which possess mutagenic ATP1 transposons (14, 15). Compound mutant mice were then crossed to the *Pdx1-Cre;LSL-Pik3ca*^{H1047R/+} line (Fig. 4A). To study ECC formation, we aged quadruple-mutant mice and observed at the humane endpoint that *piggyBac* mutagenesis led to an acceleration of *Pik3ca*-induced cancer development, reduced survival, and a shift in the tumor spectrum toward PDAC (Fig. 4B–D).

To identify transposon insertions, we performed quantitative insertion site sequencing (QISeq) of ECCs as described previously (14). We identified 38,391 nonredundant integrations with a minimal read coverage of 2 (which was set as the threshold for insertion calling). To identify genomic regions that have been hit by transposons more frequently than expected by chance, we carried out TAPDANCE (Transposon Annotation Poisson Distribution Association Network Connectivity Environment) statistical analysis (36), which identified 90 common insertion sites (CIS; Supplementary Table S1). Figure 4E shows the genome-wide distribution of these insertions and indicates CIS genes within some of the transposon insertion density peaks. Among the 90 TAPDANCE CISs, we identified four main gene clusters: (i) insertions into important regulators of PI3K signaling, such as *Pten*, *Lats1*, and *Frk*; (ii) CIS in genes that have been reported to be direct or indirect regulators of p27^{Kip1} (*Cdkn1b*) protein abundance, such as *Fbxw7* and *Ppm1b*; (iii) regulators of cell cycle and DNA replication, such as *Sfi1*, *Hdac2*, and *Hjurf*; and (iv) genes of the ubiquitin proteasome system, such as *Usp9x*, *Fbxo30*, and *Ubr5* (Fig. 4F). Most of the identified genes have not been implicated in epithelial cancer development but are interesting candidates for further analysis. *Vmp1*, for example, is a downstream target of the PI3K–Akt pathway and implicated in autophagy (37).

To identify significantly enriched interaction networks in ECC, we used the STRING database (<http://string-db.org>; ref. 38). Thereby, we confirmed enrichment of CIS gene interactions with *Pik3ca*/*Pten* and p27^{Kip1} (*Cdkn1b*) in ECC ($P = 5.43e-06$; Fig. 4G). Cross-species comparison of the top 24 CISs of the transposon screen with recurrent genetic aberrations found in human bile duct cancer revealed an overlap of 15 altered genes, including *RNF43*, *FBXW7*, *PTEN*, *FAT1*, *HDAC2*, *USP9X*, and *UBR5* (Supplementary Fig. S5).

The main insertional mutagenesis hits, and their function as direct or indirect regulators of PI3K signaling, p27^{Kip1}

abundance, and cell-cycle progression are summarized in Supplementary Fig. S6.

Functional *In Vivo* Validation of a Context-Specific Oncogenic PTEN–PIK3CA Signaling Node in ECC

More than 50% of the ECC tumors (9/17) had insertions in *Pten*. The position and orientation of the ATP1-S2 transposon, which carries a CAG promoter, a splice donor, bidirectional SV40 polyadenylation signals, and two splice acceptors, can be used to predict whether it is likely to drive or disrupt gene transcription (14, 15). Disruption of transcription may occur if the transposon inserts into a gene with no CAG promoter relative to the direction of transcription; in this situation, the gene is a putative tumor suppressor gene (TSG). Transcriptional activation may occur if the transposon is sense-oriented and upstream of the translation start site, supporting gene expression from the unidirectional CAG promoter. Analysis of transposon insertion position and orientation in the *Pten* locus revealed a random distribution and sense or antisense orientation, suggesting that gene function is disrupted (Fig. 5A).

To functionally validate *Pten* as a TSG in ECC, we used a genetic loss-of-function approach and inactivated *Pten* in the *Pdx1* lineage using floxed *Pten* mice (*Pten*^{fl/fl}; ref. 39). *Pdx1-Cre* mediated deletion of *Pten*-induced extrahepatic bile duct cancer formation in all animals of the tumor watch cohort analyzed so far (Fig. 5B–D). These findings confirm PI3K signaling as a driver of ECC development in an independent genetic model and validate our transposon screen functionally.

The inactivation of PTEN argues for the need to select for aberrant enrichment of PI3K signaling during tumor evolution. This note is underscored by the observation that several CISs in the *Pik3ca*^{H1047R} model, such as *Lats1* and *Frk/Rak*, have been shown to regulate the PI3K pathway (refs. 40, 41; Fig. 4F and G). To test genetically whether a threshold effect of PI3K signaling output is indeed a critical determinant of ECC formation *in vivo*, we increased the *Pik3ca*^{H1047R} gene dose and used homozygous *Pik3ca*^{H1047R}-mutant mice, which express the oncogene from both alleles (*LSL-Pik3ca*^{H1047R/H1047R}). This increased *Pik3ca* expression levels, PI3K signaling output, and animal mortality; shortened survival; and further shifted the tumor spectrum from PDAC toward ECC (Fig. 5C–F).

Taken together, these results provide mechanistic *in vivo* evidence that the canonical PI3K-dependent signaling pathway drives ECC formation in a gene dose-dependent manner, arguing that a certain level of PI3K signaling output strength is important for cancer formation in the extrahepatic bile duct.

p27^{Kip1} Is a Tissue-Specific Barrier of Tumor Evolution

Combining data from STRING analysis (<http://string-db.org>) of the *piggyBac* insertional mutagenesis screen and correlative data from literature reviews suggests that p27^{Kip1} (*Cdkn1b*) is an important barrier in ECC tumorigenesis and a target of several of the identified CIS genes (Fig. 4G; Supplementary Fig. S6). Overactivation of the PI3K signaling pathway through dysregulated *Pik3ca* and/or *Pten* loss, as well as alterations in *Fbxw7*, *Ppm1b*, and *Frk*, has been shown to regulate p27^{Kip1} protein expression directly or indirectly

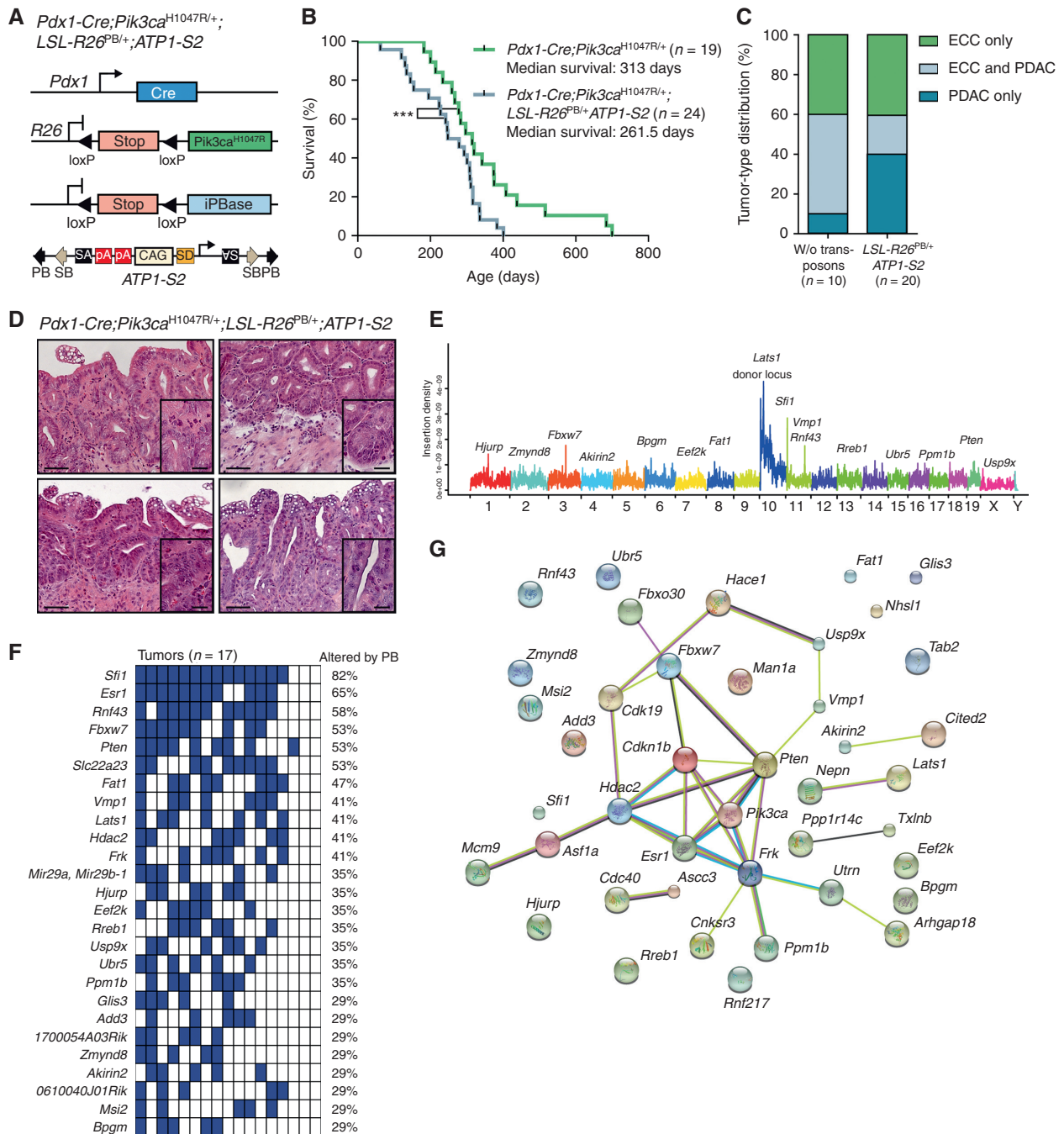


Figure 4. Identification of cancer genes in the extrahepatic biliary tract by a *piggyBac* transposon mutagenesis screen. **A**, Genetic strategy used to activate ATP1-S2 transposons by the *piggyBac* (PB) transposase in a *Pdx1-Cre;LSL-Pik3ca^{H1047R/+}*-mutant background. The ATP1-S2 mouse line carries 20 copies of the transposon construct on chromosome 10, which can be mobilized by the *piggyBac* transposase. Unidirectional integration of the transposon can lead to gene activation through its CAG promoter. Gene inactivation is independent of transposon orientation. CAG, CAG promoter; iPBBase, insect version of the *piggyBac* transposase; pA, poly adenylation site; SA, splice acceptor; SD, splice donor. **B**, Kaplan-Meier survival curves of the indicated genotypes (***, $P < 0.001$, log-rank test). The *Pdx1-Cre;Pik3ca^{H1047R/+}* cohort is the same as that shown in Fig. 2C. **C**, Tumor-type distribution according to histologic analysis of the extrahepatic bile duct and pancreas from *Pdx1-Cre;LSL-Pik3ca^{H1047R/+}* and *Pdx1-Cre;LSL-Pik3ca^{H1047R/+};LSL-R26^{PB};ATP1-S2* mice. W/o, without. **D**, Representative hematoxylin and eosin stainings of four individual *piggyBac*-induced ECC of *Pdx1-Cre;LSL-Pik3ca^{H1047R/+};LSL-R26^{PB};ATP1-S2* mice. Scale bars, 50 μ m for micrographs and 20 μ m for insets. **E**, Genome-wide representation of transposon insertion densities in ECCs (pooled data from 17 tumors). Selected CIS genes are depicted. The transposon donor locus is on chromosome 10. **F**, Co-occurrence analysis of the CIS identified by TAPDANCE analysis in 17 tumors. Each column represents one tumor where insertions in the respective genes are indicated in blue. The fraction of tumors carrying an insertion in the respective genes is given as percentage. **G**, Network of protein interactions between CIS genes generated by STRING analysis (38). Each network node represents one protein. Interactions are marked by lines in different colors (green, neighborhood evidence; purple, experimental evidence; light blue, database evidence; black, coexpression evidence). *Cdkn1b*, p27^{Kip1}.

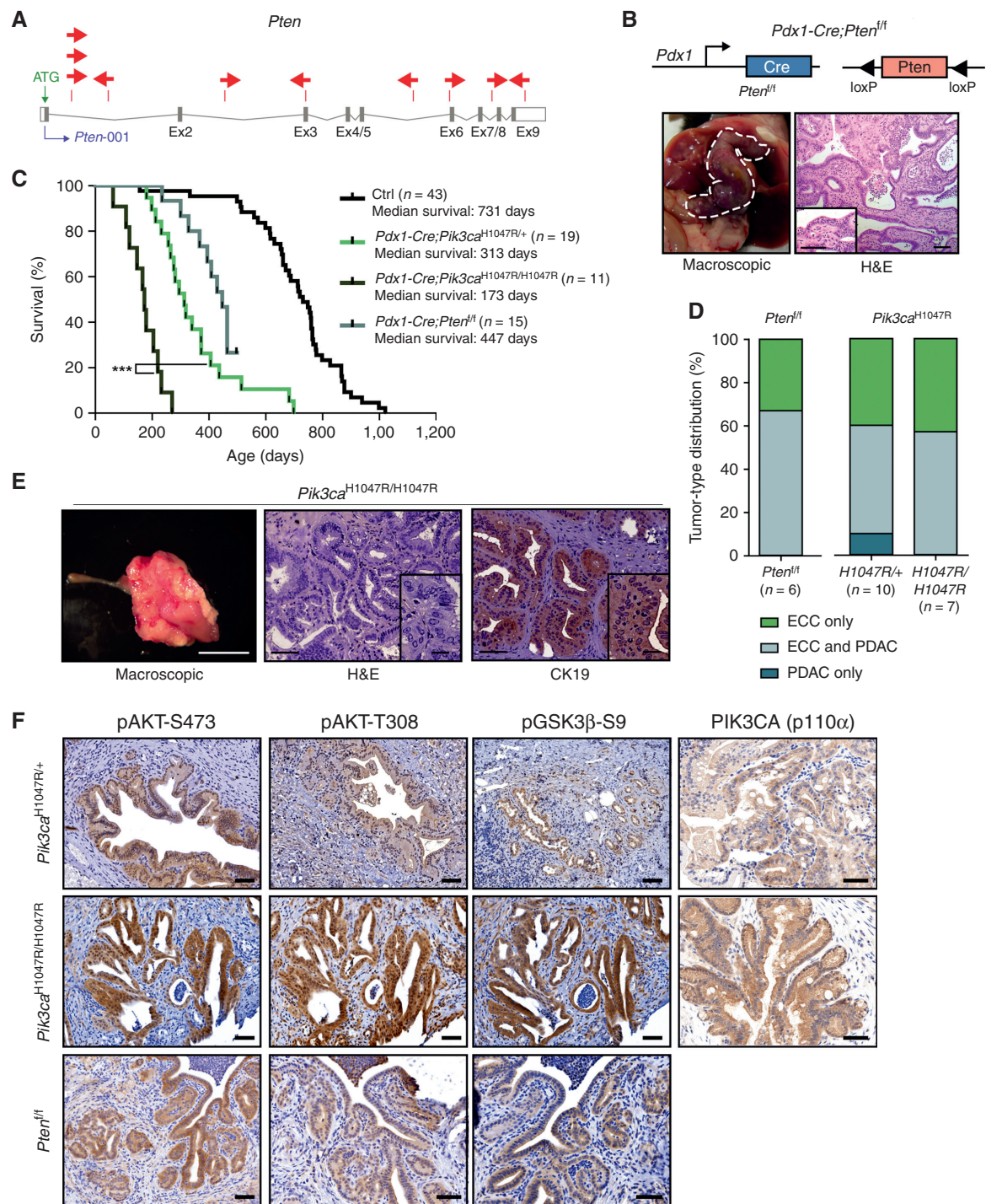


Figure 5. Functional validation of transposon integrations: PI3K signaling output is a critical determinant of ECC development. **A**, *piggyBac* insertion patterns in *Pten*. *Pten* possesses one protein-coding isoform consisting of nine exons. Each arrow represents one insertion and indicates the orientation of the CAG promoter that was introduced into the transposon. **B**, Top: genetic strategy used to inactivate *Pten* in the *Pdx1* lineage using a *Pdx1-Cre* line. Bottom: representative macroscopic picture (left, bile duct depicted by a white dashed line) and hematoxylin and eosin (H&E)-stained tissue section (right) of an ECC from a *Pdx1-Cre;Pten^{fl/fl}* mouse. Scale bars, 50 μ m for micrographs and 50 μ m for insets. **C**, Kaplan-Meier survival curves of the indicated genotypes (***) ($P < 0.001$, log-rank test). The *Pdx1-Cre;Pik3ca^{H1047R/+}* and the control cohort are the same as those shown in Fig. 2C. **D**, Tumor-type distribution according to histologic analysis of the bile duct and pancreas from *Pdx1-Cre;Pten^{fl/fl}*, *Pdx1-Cre;LSL-Pik3ca^{H1047R/+}*, and *Pdx1-Cre;LSL-Pik3ca^{H1047R/H1047R}* mice. The *Pdx1-Cre;Pik3ca^{H1047R/+}* cohort is the same as shown in Fig. 2D. **E**, Left: representative macroscopic picture of an ECC from a *Pdx1-Cre;LSL-Pik3ca^{H1047R/H1047R}* mouse. Scale bar, 1 cm. Middle and right: representative H&E-stained (middle) and IHC CK19-stained (right) tissue section of an ECC from a *Pdx1-Cre;Pik3ca^{H1047R/H1047R}* mouse. Scale bars, 50 μ m for micrographs and 20 μ m for insets. **F**, Representative H&E stainings and IHC analyses of PI3K/AKT pathway activation and *Pik3ca* (p110 α) expression in the common bile duct of *Pdx1-Cre;LSL-Pik3ca^{H1047R/+}*, *Pdx1-Cre;LSL-Pik3ca^{H1047R/H1047R}*, and *Pdx1-Cre;Pten^{fl/fl}* mice. Scale bars, 50 μ m.

(41–50). *Fbxw7*, the substrate recognition component of an SCF (SKP1–CUL1–F-box protein) E3 ubiquitin–ligase complex, for example, is inactivated as a putative TSG by missense mutations in 5% to 15% of patients with bile duct cancer (3, 51), and deletion of *Fbxw7* results in decreased p27^{Kip1} protein abundance (43). Ppmb1b, a magnesium-dependent protein phosphatase, is another positive regulator of p27^{Kip1} abundance (50), eventually via dephosphorylation of p27^{Kip1} at threonine 187 to remove a signal for proteasomal degradation, as described for Ppmb1h, another member of the Ppmb1 family (52).

As demonstrated for *Pten* (Fig. 5A), the transposon insertion pattern in *Fbxw7*, *Ppmb1b*, and *Frk/Rak* (Fig. 6A) revealed random distribution across each gene and no orientation bias, predicting that inactivation of these TSGs and positive regulators of p27^{Kip1} are the mechanisms of cancer promotion. Because p27^{Kip1} levels are significantly decreased or absent specifically in patients with ECC (53), these observations suggest that p27^{Kip1} might be an important roadblock for extrahepatic biliary cancer formation in mice and men. To test this hypothesis, we analyzed p27^{Kip1} expression levels in the extrahepatic bile duct epithelium by IHC in wild-type, *Pik3ca*^{H1047R}, and *Kras*^{G12D}-mutant animals. In contrast to oncogenic *Kras*^{G12D}, p27^{Kip1} expression was selectively and significantly downregulated by *Pik3ca*^{H1047R} (Fig. 6B and C), consistent with previous reports showing that activated PI3K signaling impairs p27^{Kip1} expression in different tissue types *in vitro* and *in vivo* (42, 54, 55). To validate these findings, we analyzed the effect of PI3K inhibition on p27^{Kip1} expression levels using primary low-passaged ECC cells derived from the *Pik3ca*^{H1047R} model. Treatment with the potent and selective pan-class I PI3K inhibitor GDC-0941 blocked protein abundance of SKP2 and surrogates of PI3K signaling, such as Akt-T308, Akt-S473, and p70-S6 kinase1-S235/236 phosphorylation, and induced p27^{Kip1} expression at the mRNA and protein levels (Fig. 6D and E). To investigate whether SKP2 regulates p27^{Kip1} protein abundance in our system, we treated primary low-passaged ECC cells with a specific SKP2 inhibitor (SKP2in C1), which blocks SKP2 substrate binding. This increased p27^{Kip1} protein expression levels in a dose-dependent manner, providing additional insights into the mechanism of PI3K-mediated p27^{Kip1} downregulation (Fig. 6F).

These data demonstrate that oncogenic PI3K signaling is an important regulator of p27^{Kip1} mRNA and protein abundance in the extrahepatic bile duct and ECC cells. To functionally analyze the role of reduced p27^{Kip1} expression for ECC formation in the extrahepatic bile duct *in vivo*, we used p27^{Kip1} knockout mice (56). Genetic deletion of one p27^{Kip1}

allele in the *Pik3ca*^{H1047R}-driven model dramatically accelerated tumor formation, shortened mouse survival to a median of 172.5 days, and further shifted the tumor spectrum from PDAC toward ECC (Fig. 7A and B). All animals in the tumor watch cohort developed invasive ECCs with a desmoplastic stromal reaction (Fig. 7C).

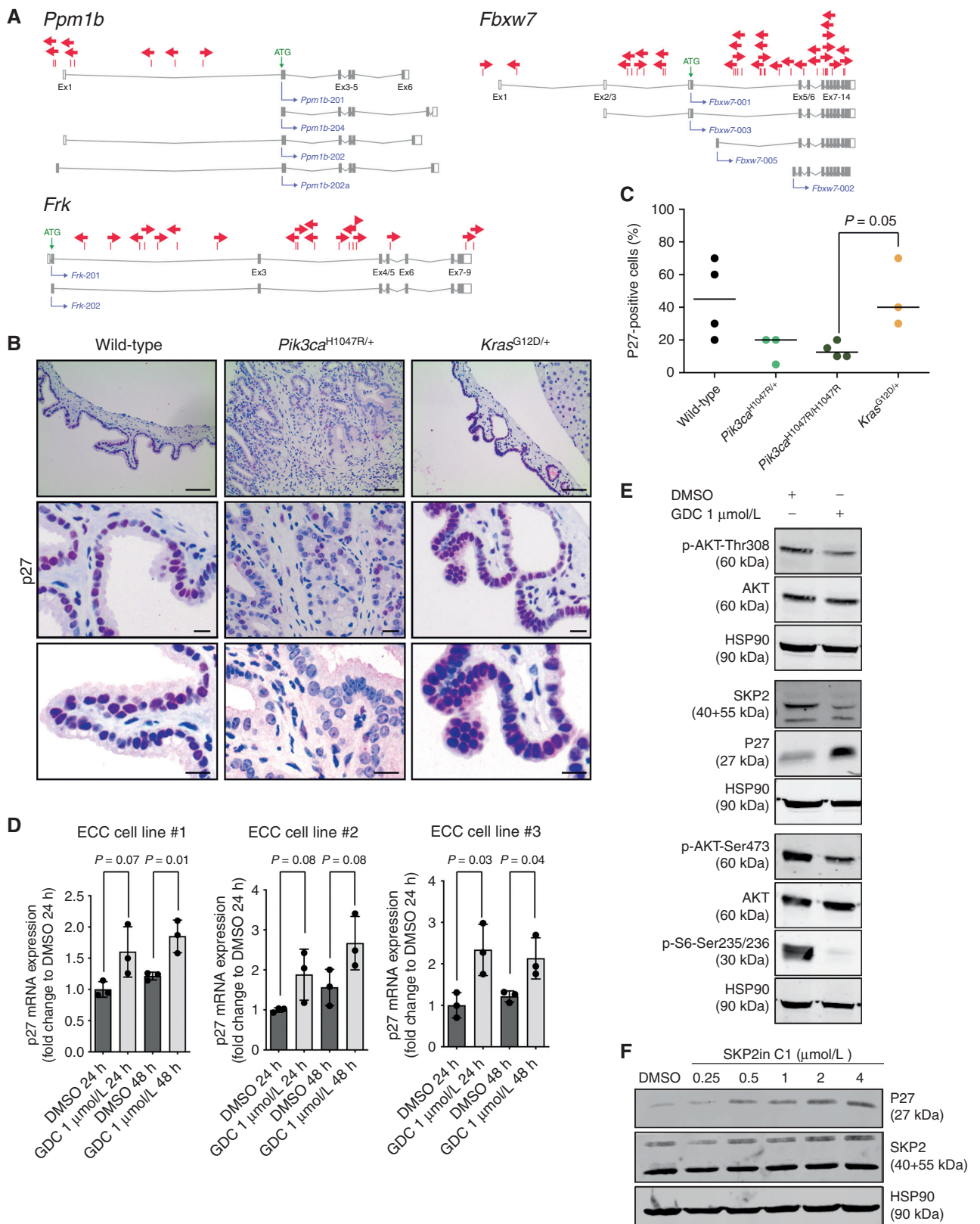
Expression of oncogenic *Kras*^{G12D} showed no effect on p27^{Kip1} protein abundance in the extrahepatic bile duct and failed to induce ECC formation (Figs. 1, 2, 6B; Supplementary Fig. S1B). To test the hypothesis of a causal relation of p27^{Kip1} as a tissue-specific roadblock for *Kras*-induced tumor formation in biliary epithelium, we deleted p27^{Kip1} in the *Pdx1-Cre;Kras*^{G12D}-driven model genetically. Inactivation of one p27^{Kip1} allele induced high-grade dysplastic lesions in the extrahepatic bile duct as well as ECC formation in some animals, a phenotype never observed in *Kras*^{G12D} mice with intact p27^{Kip1}. This reduced median survival of *Kras*^{G12D/+};p27^{Kip1+/-} mice significantly to 227 days compared with *Kras*^{G12D/+} animals with a median survival of 383 days. Homozygous p27^{Kip1} deletion led to ECC formation in all animals analyzed and further reduced median survival to 112 days (Fig. 7A–C).

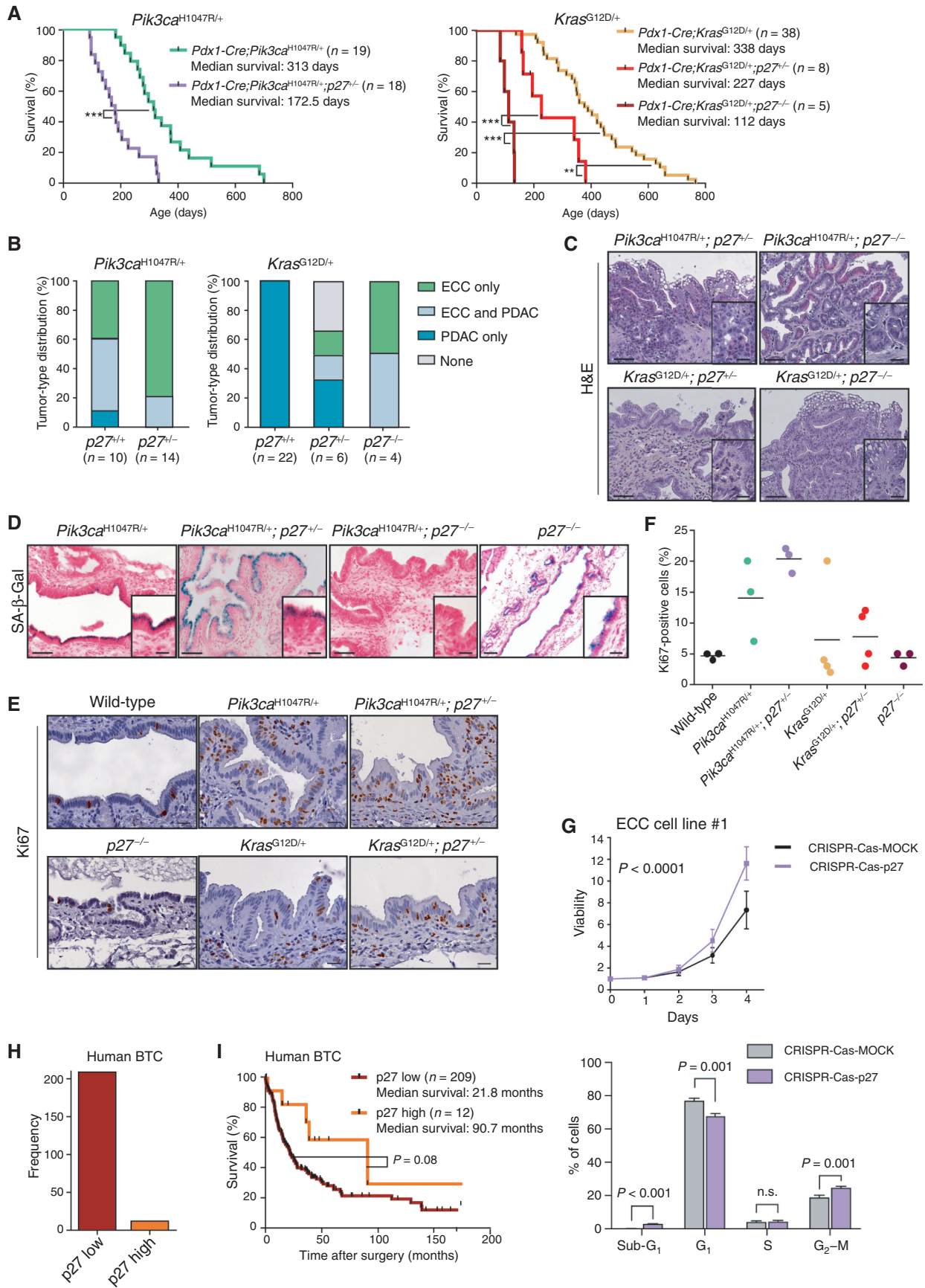
Overall, these data validate at the genetic level the notion that p27^{Kip1} is a tissue- and context-specific tumor suppressor in the extrahepatic bile duct, and contrasts with the pancreas, where p53 represents a critical tumor-suppressive barrier; furthermore, they support the view that downregulation of p27^{Kip1} is important for ECC initiation and essential for KRAS-induced transformation of the extrahepatic bile duct (Supplementary Graphical Abstract).

To investigate the transcriptional programs involved in the context-dependent regulation of the p27^{Kip1} network, we performed RNA-sequencing (RNA-seq) analysis of *Pik3ca*^{H1047R}- and *Kras*^{G12D}-driven low-passaged primary ECC and PDAC cell cultures treated for 48 hours with the PI3K inhibitor GDC-0941 or DMSO as control. We identified profound differences between *Pik3ca*^{H1047R}- and *Kras*^{G12D}-driven tumors. Whereas blockade of PI3K signaling induced significant changes to the transcriptional program of *Pik3ca*^{H1047R}-driven ECCs and PDACs (146 and 142 differentially expressed genes in ECC and PDAC, respectively), it had only minor effects on the transcriptional output of *Kras*^{G12D}-induced PDAC (22 differentially expressed genes; Supplementary Fig. S7A and S7B).

Pathway analysis of the significantly regulated genes revealed substantial changes in RNA binding, processing, splicing, and metabolism, as well as E2F targets in *Pik3ca*^{H1047R}-driven ECCs (top 10 pathways ranked by FDRq value shown in Supplementary Fig. S7C). In contrast, *Pik3ca*^{H1047R}-driven

Figure 6. p27^{Kip1} (Cdkn1b) expression is downregulated by mutant PIK3CA^{H1047R}. **A**, piggyBac insertion patterns for selected CIS genes implicated in p27^{Kip1} (Cdkn1b) regulation. *Ppmb1b* and *Fbxw7* possess four protein-coding transcripts. *Frk* has two protein-coding isoforms consisting of eight and nine exons. Each arrow represents one insertion and indicates the orientation of the CAG promoter that was introduced into the transposon. **B**, Representative IHC analysis of p27^{Kip1} expression in the common bile duct of 6-month-old wild-type, *Pdx1-Cre;LSL-Pik3ca*^{H1047R/+}, and *Pdx1-Cre;LSL-Kras*^{G12D/+} mice. Scale bars, 80 μm (top) and 20 μm (middle and bottom). IHC staining was performed using 3-amino-9-ethylcarbazole (AEC) as chromogen, resulting in a pink color of positively stained cells. **C**, Quantification of p27^{Kip1}-positive bile duct epithelial cells in 6-month-old wild-type, *Pdx1-Cre;LSL-Pik3ca*^{H1047R/+}, *Pdx1-Cre;LSL-Pik3ca*^{H1047R/H1047R}, and *Pdx1-Cre;LSL-Kras*^{G12D/+} mice ($n = 3–4$ animals per genotype). Each dot represents one animal; the horizontal line represents the mean ($P = 0.05$, *Pdx1-Cre;LSL-Pik3ca*^{H1047R/H1047R} vs. *Pdx1-Cre;LSL-Kras*^{G12D/+}, Wilcoxon rank sum test). **D**, qRT-PCR analysis of p27^{Kip1} mRNA expression in three primary murine ECC cell lines from *Pdx1-Cre;LSL-Pik3ca*^{H1047R/+} mice treated with either vehicle (DMSO) or 1 μmol/L GDC-0941 (GDC) for 24 or 48 hours (h) as indicated. Data are shown as fold change to DMSO treatment ($n = 3$; mean + SD; P values are indicated, Student t test). **E**, Immunoblot analysis of PI3K/AKT pathway activation and p27^{Kip1} expression in primary murine ECC cell line #1 treated with either vehicle (DMSO) or 1 μmol/L GDC-0941 for 48 hours. Hsp90α/β was used as loading control. **F**, Immunoblot analysis of p27^{Kip1} expression in primary murine ECC cell line #1 treated with either vehicle (DMSO) or the indicated concentrations of the SKP2 inhibitor SKP2in C1 for 48 hours. Hsp90α/β was used as loading control.





PDAC showed mainly changes of metabolic pathways and the mitochondrion upon PI3K pathway perturbation. E2F transcription factors (TF) have previously been shown to regulate p27^{Kip1} abundance via the transcriptional regulation of SKP2. Therefore, the observed E2F target gene signature provides evidence that a PI3K-induced E2F node regulates p27^{Kip1} abundance via SKP2, which is downregulated at the mRNA and protein levels upon GDC-0941 treatment (Fig. 6E; Supplementary Fig. S7D) and regulates p27^{Kip1} protein abundance in ECC cells (Fig. 6F). Accordingly, the Biocarta p27 pathway is significantly altered in *Pik3ca*^{H1047R}-driven ECC cells upon GDC-0941 treatment (Supplementary Fig. S7D). For *Kras*-driven PDAC, we could not detect any significantly altered pathway, because of the low number of significantly differentially expressed genes. These findings support the view that PI3K pathway activation by oncogenic *Kras*^{G12D} does not reach a critical threshold that is necessary to alter the p27 network and downregulate p27^{Kip1} protein abundance, which is necessary for ECC induction.

To gain more insights into the context-specific transcriptional control of the p27^{Kip1} network under basal conditions, we analyzed the top 10 differentially targeting TFs in *Pik3ca*^{H1047R}-driven ECC and *Kras*^{G12D}-induced PDAC. We observed fundamental differences in p27^{Kip1} network regulation and identified context-specific TFs that control the p27^{Kip1} tumor suppressor node specifically in ECC (Supplementary Fig. S7E).

To analyze p27^{Kip1} function in the extrahepatic biliary epithelium, we investigated early events of tumorigenesis. Surprisingly, p27^{Kip1} inactivation triggered senescence of the normal biliary epithelium in the absence of an oncogene. In contrast, it bypassed OIS in the context of *Pik3ca*^{H1047R}-induced early neoplastic BilIN lesions (Fig. 7D; Supplementary Graphical Abstract). Importantly, these BilIN lesions showed concomitant increased proliferation rates as evidenced by Ki67 IHC *in situ* (Fig. 7E and F). CRISPR-Cas9-mediated deletion of p27^{Kip1} in primary low-passaged ECC cells derived from the *Pik3ca*^{H1047R} model induced cell proliferation and cell-cycle progression (Fig. 7G; Supplementary Fig. S8A and S8B).

These results provide evidence that canonical p27^{Kip1} tumor suppressor functions, which regulate G₀ to M phase cell-cycle transitions, contribute significantly to the observed effects, although the importance of additional and alternate effectors of p27^{Kip1} cannot be completely excluded (42).

To further substantiate our hypothesis that p27^{Kip1} is also a roadblock in human BTC, we analyzed p27^{Kip1} expression in 221 primary surgically resected tumor specimens. In accordance with the murine *in vivo* studies, we observed weak or absent p27^{Kip1} expression in nearly all human BTC (weak or absent p27^{Kip1}: *n* = 209; strong p27^{Kip1}: *n* = 12) specimens (Fig. 7H). In addition, tumors with weak or absent p27^{Kip1} expression were associated with poor survival. Kaplan-Meier curves comparing p27^{Kip1} expression with survival showed a trend toward separation (*P* = 0.08, log-rank test; Fig. 7I). This is in accordance with previous studies reporting that p27^{Kip1} protein abundance is an independent predictor of survival for patients with CC (53, 57–59).

DISCUSSION

There have been no major improvements in the treatment of ECC in the last three decades, and no effective targeted therapies are available (1–3). Next-generation sequencing and molecular tumor profiling uncovered a plethora of potentially actionable molecular alterations associated with ECC malignancy (3, 13, 19–23). However, despite these exciting new data describing the genomic landscape of ECC, we are far from understanding the functional consequences of these genetic alterations and the underlying tumor biology. This is due to (i) the inherent limitations of current cancer genome analysis to distinguish driver and passenger mutations and to predict the functional consequences of missense mutations, (ii) the often descriptive nature of such data, (iii) the complexity of signaling processes and tumor suppressor barriers downstream of altered genes, (iv) context-specific differences between different cancer entities, (v) tumor heterogeneity, and (vi) a lack of understanding of signals from the tumor micro- and macroenvironment. Thus, there is an urgent need for complementary functional studies using informative and predictive model systems, which fill the gap between the genetic landscape and the largely unknown biology of ECC (2, 3). This offers the best means of identifying novel therapeutic approaches for ECC that are robust and effective in the clinic (60, 61).

GEMMs have been developed for diverse cancer types in the last two decades that faithfully recapitulate the histologic, molecular, genetic, and clinical hallmarks of the human disease (60). They are often based on the Cre/loxP system and

Figure 7. p27^{Kip1} is a context-specific roadblock for *Kras*-induced ECC formation. **A**, Kaplan-Meier survival curves of the indicated genotypes (***, *P* < 0.001; **, *P* < 0.01, log-rank test). **B**, Tumor type distribution according to histologic analysis of the extrahepatic bile duct and pancreas from *Pdx1-Cre; LSL-Pik3ca*^{H1047R/+} and *Pdx1-Cre;LSL-Pik3ca*^{H1047R/+};p27^{-/-} mice (left) and *Pdx1-Cre;LSL-Kras*^{G12D/+}; *Pdx1-Cre;LSL-Kras*^{G12D/+};p27^{-/-}, and *Pdx1-Cre; LSL-Kras*^{G12D/+};p27^{-/-} animals (right). Significant increase of ECC development in mice with the *Pdx1-Cre;LSL-Kras*^{G12D/+};p27^{-/-} genotype (*P* < 0.0001, Fisher exact test). **C**, Representative hematoxylin and eosin (H&E) staining of the common bile duct of aged *Pdx1-Cre;LSL-Pik3ca*^{H1047R/+};p27^{-/-}, *Pdx1-Cre; LSL-Pik3ca*^{H1047R/+};p27^{-/-}, *Pdx1-Cre;LSL-Kras*^{G12D/+};p27^{-/-}, and *Pdx1-Cre;LSL-Kras*^{G12D/+};p27^{-/-} mice. **D**, Representative SA-β-Gal staining of the common bile duct of *Pdx1-Cre;LSL-Pik3ca*^{H1047R/+}, *Pdx1-Cre;LSL-Pik3ca*^{H1047R/+};p27^{-/-}, *Pdx1-Cre;LSL-Pik3ca*^{H1047R/+};p27^{-/-}, and p27^{-/-} mice. **C** and **D**, Scale bars, 50 μm for micrographs and 20 μm for insets. **E**, Representative images of Ki67-stained common bile duct tissue sections of 3-month-old wild-type (control), *Pdx1-Cre;LSL-Pik3ca*^{H1047R/+};p27^{-/-}, *Pdx1-Cre;LSL-Pik3ca*^{H1047R/+};p27^{-/-}, p27^{-/-}, *Pdx1-Cre;LSL-Kras*^{G12D/+}, and *Pdx1-Cre;LSL-Kras*^{G12D/+};p27^{-/-} mice. Scale bars, 20 μm. **F**, Quantification of Ki67-positive biliary epithelial cells of indicated genotypes. Each dot represents one animal, and the horizontal line represents the mean. **G**, Top: viability assay of primary murine ECC cell line #1 from a *Pdx1-Cre;LSL-Pik3ca*^{H1047R/+} mouse after CRISPR-Cas9-mediated deletion of p27^{Kip1} (*Cdkn1b*). Cells were transfected with either Cas9-sgRNA-p27^{Kip1} targeting *Cdkn1b* (CRISPR-Cas-p27) or a MOCK Cas9-sgRNA-MOCK vector, selected using puromycin, and cell viability was measured in triplicate using the MTT assay (*n* = 4 independent experiments; mean ± SD; *P* < 0.0001, two-way ANOVA). Bottom: FACS-based cell-cycle analysis of the cells shown in the top panel. The *P* values were determined with multiple *t* tests and Benjamini correction and are shown in the figure. n.s., not significant. **H**, Quantification of p27^{Kip1} expression by IHC of 221 surgically resected human BTC specimens. **I**, Kaplan-Meier survival curves of patients with BTC with low or high p27^{Kip1} protein abundance (*P* = 0.08, log-rank test). The *Pdx1-Cre; Pik3ca*^{H1047R/+} and *Pdx1-Cre;LSL-Kras*^{G12D/+} cohorts shown in **A** and **B** are the same as those shown in Fig. 2C and D.

tissue-specific expression of oncogenes and/or deletion of TSGs (62). Such conditional models have provided important information about the natural biology of many cancer types and revealed potential targets for early detection and therapeutic intervention (61, 63). Accordingly, they have become one of the gold standards for preclinical investigation of novel lead compounds and therapeutic regimes (60, 61).

For ECC research, many sophisticated tools of fundamental importance, such as conditional GEMMs, have not been developed so far. This represents a major bottleneck, which is rate limiting for preclinical research and explains in part the poor molecular understanding of this devastating disease (1, 12, 19). We addressed this limitation and developed novel GEMMs of oncogenic KRAS- and PI3K-driven ECC subtypes that exhibit hallmarks of the human disease—from multi-stage BilIN precursor lesion progression to invasive stroma-rich ductal adenocarcinomas (see Supplementary Graphical Abstract for an overview of the models).

The pathogenesis of human ECC is a complex process involving alterations in the activity of multiple oncogenes and TSGs and their downstream effector pathways (1, 3, 64). Of these, activation of RAS and PI3K signaling pathways represents the most frequent events (3). Our new autochthonous ECC models offer for the first time the possibility to (i) study the biology of these molecular cancer subtypes and their associated pathways, (ii) discover and validate therapeutic targets, and (iii) provide the context for preclinical trials to find new ways to treat ECC subtypes and identify biomarkers of response and resistance.

We used the novel *Pik3ca*^{H1047R}-driven GEMM of ECC to perform a large genome-wide unbiased functional transposon-based mutagenesis screen to discover cooperating cancer genes in ECC. Using the *piggyBac* transposition system, we identified many novel cancer genes and cancer-driving networks. Some of them specifically feed into the PI3K pathway, such as inactivation of *Pten* or *Lats1*, or drive inactivation of the tumor suppressor *p27^{Kip1}* (*Cdkn1b*), which we identified as a major roadblock for ECC pathogenesis. Subsequently, we validated the essential role of PI3K signaling output strength and *p27^{Kip1}* downregulation for ECC formation *in vivo* using *Kras*^{G12D}- and *Pik3ca*^{H1047R}-driven GEMMs with genetic alteration in these pathways (please see Supplementary Graphical Abstract for an overview of the tissue-specific tumor suppressor barriers of ECC formation).

p27^{Kip1} is a cyclin-dependent kinase (CDK) inhibitor and one of the most frequently misregulated proteins in human cancers. It is an atypical TSG, as it is rarely mutated or deleted; rather, *p27* protein levels are reduced or the protein is mislocalized, which promotes uncontrolled cell growth (42). Our data suggest that a certain level of PI3K output is necessary to block *p27^{Kip1}* expression to a level that allows extrahepatic bile duct cancer formation. To test this hypothesis, we over-activated the PI3K pathway *in vivo* and observed decreased *p27^{Kip1}* levels and accelerated ECC formation. In line with this, genetic manipulation of *p27^{Kip1}* (*Cdkn1b*) expression using knockout mice validated its role as a roadblock for ECC pathogenesis in the PI3K-driven model. In contrast to *Pik3ca*^{H1047R}, activation of oncogenic *Kras*^{G12D} induced tumor development only in the pancreas but completely failed to drive ECC. However, deletion of *p27^{Kip1}* (*Cdkn1b*) enabled

Kras-driven tumorigenesis in the extrahepatic bile duct with high penetrance. Because the TSG *p27^{Kip1}* is tightly linked to PI3K signaling (42, 54, 55), our genetic *in vivo* data show for the first time that a PI3K-*p27^{Kip1}* node is an essential determinant of PI3K- as well as *Kras*-driven ECC development (see Supplementary Graphical Abstract). This has important therapeutic implications, because several pharmacologic inhibitors directed against the PI3K pathway are under clinical investigation and drugs that combat *p27^{Kip1}* dysfunction are currently under development (48, 65).

Our data allow for two important conclusions. First, the response and vulnerability to distinct oncogenic drivers, allowing or preventing cancer development at different anatomical sites, are strictly tissue-specific, even if the different tissue types have a common developmental origin and indistinguishable morphology, as shown for the extrahepatic bile duct and the pancreatic duct. Second, distinct tumor suppressor barriers and signaling thresholds are operative in different tissue types even in the presence of the same initial oncogenic lesion as shown for *Kras*^{G12D} and *p27^{Kip1}* in the extrahepatic bile duct and the pancreas. Thus, our results demonstrate that tissue-specific mechanisms contribute significantly to the context-specific oncogenic potency of a cancer driver and support the view that each tissue has its own unique signaling requirement during oncogene-induced transformation. This provides *in vivo* evidence for the rationale to investigate KRAS- and PI3K-driven oncogenic pathways in a strictly tissue- and context-specific manner to characterize the relevant nodes engaged in different tumor entities. Tissue context is an important determinant of treatment response and resistance. Therefore, the advance in our understanding of tissue-specific effects of oncogenic *Kras* and PI3K signaling presented here will affect clinical practice in the future because it clearly shows that results obtained in one tumor entity cannot simply be extrapolated to another.

In conclusion, our findings establish cell context-specific functions for KRAS and PI3K signaling and engagement of *p27^{Kip1}* in transformation of the extrahepatic bile duct that are independent of the p53 pathway. They also suggest that the role of oncogenic drivers varies depending on the cell and tissue type and microenvironment. Our findings underscore that tissue context is an important determinant of tumorigenesis. A deeper understanding of the molecular mechanisms involved in ECC pathogenesis and tumor biology will provide novel therapeutic targets and biomarkers of response essentially needed for clinical decision-making and the design of novel and improved next-generation targeted treatment regimens for patients with ECC.

METHODS

Mouse Strains and Tumor Models

Pdx1-Cre (16), *LSL-R26^{tdTomato}/+* (17), *R26^{mT-mG}/+* (18), *LSL-Pik3ca*^{H1047R/+} (24), *LSL-Kras*^{G12D/+} (16), *Trp53^{f/f}* (35), *p27^{-/-}* (56), *LSL-R26^{6B}/+* (14), *ATP1-S2* (15), and *Pten^{f/+}* (39) alleles have been previously described. All animal studies were conducted in compliance with European guidelines for the care and use of laboratory animals and were approved by the Institutional Animal Care and Use Committees of Technische Universität München, Regierung von Oberbayern, and

UK Home Office. Animals on a mixed C57Bl6/129S6 genetic background were intercrossed to obtain the desired genotype, and both male and female mice with the correct genotype were aged to assess cancer formation and survival of the animals. Wild-type and animals containing only Cre recombinase served as controls as indicated in the figure legends. Sequence information of genotyping PCR primers is given in the Supplementary Methods.

Materials

Cell culture reagents were obtained from Thermo Fisher Scientific. Primers were made by Eurofins Genomics, and restriction endonucleases were obtained from New England Biolabs. The *Escherichia coli* strain Stbl3 (Thermo Fisher Scientific) was used for transformation and plasmid amplification. The PI3K inhibitor GDC-0941 free base was purchased from LC Laboratories. The SKP2 inhibitor SKP2in C1 was purchased from Selleckchem.

White Light and Fluorescence Stereomicroscopy

Macroscopic pathologic analysis of murine tissues including ECC and PDAC was performed, and white-light and fluorescence pictures were taken using a Zeiss Stemi 11 fluorescence stereomicroscope (Zeiss).

Histopathology and IHC

Mouse tissue specimens were fixed in 4% buffered formalin overnight, embedded in paraffin, and sectioned (2 μ m thick). Murine PanIN lesions and PDAC were graded according to the established nomenclature (66). Murine BilIN were graded in analogy to the human classification (27, 67). The normal common bile duct in mice is morphologically similar to its human counterpart. It is lined by a single layer of uniform cuboidal cells and accompanied by small peribiliary glands. Proliferative lesions with a flat or micropapillary structure composed of tall columnar cells with some loss of cellular polarity and/or nuclear pseudostratification with mild nuclear abnormalities (i.e., slight hyperchromasia or irregular nuclear membrane) were categorized as low-grade BilIN. High-grade BilIN were defined as lesions with micropapillary architecture and diffuse loss of cellular polarity, “budding off” of single epithelial cells into the lumen and severe cellular and nuclear pleomorphism. By definition, invasion through the basement membrane had to be absent in these strictly intraepithelial lesions. The examiner was blinded to the genotype of the animals.

For immunodetection, formalin-fixed, paraffin-embedded tissue sections were dewaxed, rehydrated, and placed in a microwave (10 minutes, 600 watt) in unmasking solution H-3300 (Vector Laboratories) to recover antigens. Sections were incubated with primary pERK (p44/42; #4376; 1:1,000; RRID:AB_331772), cleaved caspase-3 (#9664; 1:150; RRID:AB_2070042), PIK3CA (p110 α ; #4249; 1:400; RRID:AB_2165248), pAKT-T308 (#2965; 1:50; RRID:AB_2255933), pAKT-S473 (#4060; 1:50; RRID:AB_2315049), pGSK3 β -S9 (#9323; 1:100; RRID:AB_2115201; all from Cell Signaling Technology), p21 (sc-397-G; 1:50; RRID:AB_632127; Santa Cruz Biotechnology), p53 (CMS; 1:300; RRID:AB_2744683; Novocastra/Leica Mikrosysteme), p27^{Kip1} (ab62364; 1:500; RRID:AB_944575; Abcam), and Ki67 (SP6; 1:50; RRID:AB_2722785; DCS Diagnostics) antibodies followed by a secondary antibody conjugated to biotin (Vector Laboratories). Antibody detection of pERK, cleaved caspase-3, and PIK3CA (p110 α) was performed with the Bond Polymer Refine Detection Kit (Leica). Images were acquired using Leica AT2 Scanner (Leica). Quantification of p27^{Kip1}, cleaved caspase-3, and Ki67-positive cells was performed by exclusively counting epithelial cells in at least 10 high-power fields in at least three animals, and the examiner was blinded to the genotype of the animals.

SA- β -Gal Staining

SA- β -Gal staining of cryosections was performed with the Senescence β -Galactosidase Staining Kit in accordance with the manufacturer's protocol (Cell Signaling Technology). Counterstaining was carried out with nuclear fast red. Images were acquired using Aperio Versa Scanner (Leica).

Immunofluorescence and Confocal Laser-Scanning Microscopy

Tissues were fixed in 4% buffered formalin for 2 hours, dehydrated at 4°C (15% sucrose in PBS for 4 hours; 30% sucrose in PBS overnight), and embedded in Tissue-Tek (Sakura) before being frozen in liquid nitrogen. 20- μ m thick frozen sections were post-fixed for 1 minute in 4% buffered formalin, washed twice in PBS, and incubated for 1 hour in PBS with 3% (w/v) bovine serum albumin (BSA), 1% (w/v) saponin, and 1% (v/v) Triton-X 100. Subsequently, slides were incubated with CK19 primary antibody (ab52625, 1:100, RRID:AB_2281020, Abcam) and a DyLight 680-conjugated secondary antibody (#5366, 1:100, RRID:AB_10693812, Cell Signaling Technology). Nuclei were counterstained with TOPRO-3-iodide (1:1,000, Thermo Fisher Scientific). Sections were examined on a Leica TCS SP5 DMI 6000 CS confocal laser-scanning microscope using a 40/1.25 oil-immersion objective (Leica Microsystems).

Human BTC Tissue Samples

This study conformed to the Declaration of Helsinki and was approved by the ethics committee of the Universität Heidelberg. Written informed consent was obtained from all patients. The use of the tissue for this study was approved by the institutional ethics committee (206/05). Our cohort comprised 221 patients with CC. All tumors were resected between 1995 and 2010 at the University Hospital in Heidelberg, Germany. Neoadjuvant radiotherapy and/or chemotherapy was not applied in any of the patients. One hundred twenty-three (55.7%) patients were male, and 98 (44.3%) were female. Mean age at diagnosis was 64.7 years (range, 33.5–91.6 years). Twenty-seven (12.2%) tumors were classified as pT1, 116 (52.5%) as pT2, 61 (27.6%) as pT3, and 17 (7.7%) as pT4. One hundred fifty-one (68.3%) of the patients received concomitant lymph node resection. Of these, 83 (55%) were pN1 and 68 (45%) were pN0. Nineteen (8.6%) patients had distant metastasis at the time of resection. Fifty-seven (25.8%) of the tumors were ICCs, 94 (42.5%) were ECCs, and 70 (31.7%) were gallbladder carcinomas. Follow-up data were available for 191 patients (86.4%). The mean follow-up time of patients alive at the endpoint of analysis was 45.7 months. One hundred twenty-five (65.4%) patients died during follow-up.

Evaluation of the Human BTC Cohort

From all 221 CCs, 3- μ m sections were cut and stained with hematoxylin and eosin. Representative areas from the tumor center and invasive margins were marked by two pathologists with a special expertise in CC pathology (B. Goepfert and W. Weichert). For each case, tumor tissue cores (1.5 mm diameter) from the selected representative tumor areas were punched out of the sample tissue blocks and embedded into a new paraffin array block using a tissue microarrayer (Beecher Instruments). For the detection of p27^{Kip1}, a monoclonal mouse IgG antibody directed against p27^{Kip1} [BD Biosciences; clone: 57/Kip1/p27 (RUO); #610242; 1:100 dilution, RRID:AB_397637] was used. Bound antibody was detected with the Dako K5003 AEC kit (Dako). To exclude cases with only faint and focal putatively biologically irrelevant p27^{Kip1} expression from the p27^{Kip1} “positive” group, cases were only scored as positive when a clearly distinguishable nuclear signal of at least moderate intensity was seen in more than 50% of tumor cells.

Mapping of Transposon Insertion Sequences to the Mouse Genome and Identification of CISs

Genomic DNA was isolated from fresh-frozen ECC samples with the QIAamp DNA Mini Kit according to the manufacturer's protocol. Amplification of the transposon insertion sites and next-generation sequencing on an Illumina MySeq desktop sequencer was performed as described (14). Transposon insertion sites with a coverage of two or more reads were subjected to TAPDANCE analysis to identify nonredundant CISs (36). Network analysis was conducted with STRING (38).

Generation and Cultivation of Primary Low-Passaged Dispersed Murine ECC and PDAC Cell Cultures

Primary dispersed murine ECC and PDAC cell cultures were established from *Pdx1-Cre;LSL-Pik3ca^{H1047R/+}* and *Pdx1-Cre;LSL-Kras^{G12D/+}* mice, and cultivated as previously described (68). Cell viability was quantified by MTT assay using the substrate 3-[4,5-dimethylthiazol-2-yl]-2,5-diphenyltetrazolium bromide (Sigma-Aldrich Chemie). All cell lines were authenticated by genotyping and tested negative for *Mycoplasma* contamination by an inhouse PCR-based *Mycoplasma* detection assay every two months. The low-passaged cell cultures were cultivated for a maximum of 20 passages and typically used for the experiments between passages 5 and 10.

Drug Treatment

Cells were seeded in a 10-cm dish and treated 24 hours later with GDC-0941 or SKP2in C1 at the indicated concentrations or vehicle for 24 or 48 hours as indicated. The medium containing either the drug or the vehicle was changed after 24 hours.

Gene-Expression Profiling and Analysis

RNA was isolated with the RNeasy kit (Qiagen) from 80% confluent primary cells and immediately transferred into RLT buffer (Qiagen) containing β -mercaptoethanol.

RNA-seq library preparation was performed as previously described (69). Analyses were carried out using R version 3.6.2 and Bioconductor version 3.1. Differential gene-expression analysis was performed using DESeq2 version 1.26.0. A gene was considered to be differentially expressed with a Benjamini-Hochberg adjusted *P* value of 0.05 and an absolute fold change >0.5. The overrepresentation analysis was performed with MSigDB v7.1 gene sets provided by the Broad Institute, Massachusetts Institute of Technology, and Harvard University.

RNA-seq data have been deposited in the ArrayExpress database at EMBL-EBI (www.ebi.ac.uk/arrayexpress) under accession number E-MTAB-10515.

To investigate the tissue-specific regulatory networks of the p27^{Kip1} pathway, we used PANDA. PANDA integrates multiple types of data including protein-protein interactions (PPI) and gene expression to infer interaction between TFs and their target genes (70). We used the netZooR implementation of PANDA (version 0.9) to infer two separate regulatory networks for *Pik3ca^{H1047R}*-driven ECC and *Kras^{G12D}*-driven PDAC. For each network, we used the same TF/target prior and PPI networks and normalized tissue-specific gene-expression data. The TF/gene priori was downloaded from <https://sites.google.com/a/channing.harvard.edu/kimberlyglass/tools/resources>. The PPI network was downloaded from STRINGdb, integrated in the netZooR library. The resulting networks allowed us to analyze the behavior of 441 TFs, >18,000 genes, and more than 8 million weighted edges between them. The visualization of the p27^{Kip1}-related subnetworks was done in Cytoscape (v3.8.2, <https://cytoscape.org>).

CRISPR-Cas9-Mediated p27^{Kip1} Deletion in Primary Murine ECC Cell Lines

Two different sgRNAs targeting exon 1 of the *Cdkn1b* (p27^{Kip1}) gene were designed using the online tool CRISPR Design (<http://crispr.mit.edu/job/4733254127165968,1.8.2014>). The Cas9 expression vector pSpCas9(BB)-2A-Puro (pX459; Addgene plasmid #48139; www.addgene.org) was used to insert either the annealed sgRNA1 or sgRNA2 both targeting *Cdkn1b* (p27^{Kip1}). Sequence information of the sgRNAs is provided in the Supplementary Methods. Primary low-passaged murine ECC cells were cotransfected with the two modified versions of pX459 containing either sgRNA1 or sgRNA2 using Lipofectamine 2000 reagent according to the manufacturer's protocol (Invitrogen). For MOCK cells, cell lines were transfected with a modified version of the Cas9 nickase expression vector pSpCas9n(BB)-2A-Puro (pX462; Addgene plasmid #48141; www.addgene.org) containing only sgRNA1. Transfected cells were selected 24 hours later by addition of puromycin to the culture medium (2.5 μ g/mL). Cell viability of passaged cell lines was determined daily for 96 hours by MTT assay, or cell proliferation was assessed by cell counting.

Quantitative Reverse-Transcriptase PCR

Total RNA was isolated from primary ECC cell lines using the RNeasy kit (Qiagen) following the manufacturer's instructions and reverse transcribed (Thermo Fisher Scientific). Relative mRNA quantification using cyclophilin as reference gene was performed by real-time PCR analysis (TaqMan, PE Applied Biosystems). Sequence information of the qRT-PCR primers is provided in Supplementary Methods.

Cell-Cycle Analysis by Flow Cytometry

To synchronize the cell cultures, cells were seeded in 10-cm dishes in growth medium with 10% FCS overnight. The cultures were then washed by PBS and changed to serum-free medium. After 24 hours of serum starvation, the cells were passaged and released into cell cycle by the addition of serum for 6 hours. Cells were trypsinized and washed two times with PBS followed by fixation in 1 mL cold 70% EtOH. The EtOH was removed after 24 hours, and cells were washed with PBS. Cells were stained with DAPI (Sigma, 1:6,000) and acquired using Cytoflex LX (Beckman Coulter). Flow cytometry data were analyzed using FlowJo software (Version 10.6.2).

Preparation of Total Cell Lysates and Immunoblotting

Whole-cell lysates were prepared, and isolated proteins were separated in SDS-polyacrylamide gels, transferred to polyvinylidene difluoride membranes, and incubated at 4°C overnight with the following primary antibodies: pAKT-T308 (#2965, RRID:AB_2255933), pAKT-S473 (#4060, RRID:AB_2315049), pan-AKT (#4691, RRID:AB_915783), p-S6-S235/236 (#4858, RRID:AB_916156; all from Cell Signaling Technology) and p27^{Kip1} (sc528, RRID:AB_632129), Skp2 (sc7164, RRID:AB_2187650), and Hsp90 alpha/beta (sc13119, RRID:AB_675659; all from Santa Cruz Biotechnology). Primary antibodies were followed by Alexa680-coupled secondary antibodies (Thermo Fisher Scientific) and detected by the Odyssey Infrared Imaging System (Licor).

Data Analysis

Unless otherwise indicated, all data were determined from at least three independent experiments and expressed as mean values \pm SEM. GraphPad Prism (versions 5 and 8) was used for graphical presentation of the data and calculation of statistical tests except for the Wilcoxon rank sum test. The Wilcoxon rank sum test was computed in R Language. Statistical tests and *P* values are provided in the figure legends. Values of *P* = 0.05 or less were considered to be statistically significant.

Authors' Disclosures

K. Steiger reports other support from Roche and TRIMT outside the submitted work, as well as a patent for radiopharmaceutical issued. S. Roessler reports grants from German Cancer Aid, German Research Foundation, and PSC Partners Seeking a Cure Foundation outside the submitted work. A. Bradley reports other support from Kymab outside the submitted work. M. Reichert reports personal fees from Roche, Celgene, and Falk outside the submitted work. W. Weichert reports personal fees from Roche, MSD, Bristol Myers Squibb, AstraZeneca, Pfizer, Merck, Lilly, Boehringer, Novartis, Takeda, Bayer, Amgen, Astellas, Eisai, Illumina, Siemens, Agilent, ADC, GlaxoSmithKline, and Molecular Health and grants from Roche, MSD, Bristol Myers Squibb, and AstraZeneca outside the submitted work. O.J. Sansom reports grants from Novartis, AstraZeneca, and Cancer Research Technology; personal fees from Boehringer Ingelheim; and other support from Ionctura outside the submitted work. J.P. Morton reports grants from CRUK during the conduct of the study, as well as grants from Cancer Research UK, Pancreatic Cancer UK, and Medical Research Council outside the submitted work. G. Schneider reports grants from Deutsche Forschungsgemeinschaft and German Cancer Consortium (DKTK) during the conduct of the study. D. Saur reports grants from Deutsche Forschungsgemeinschaft (DFG SA 1374/4-3 and SFB 1321 Project-ID 329628492), European Research Council, and German Cancer Consortium during the conduct of the study, as well as personal fees and nonfinancial support from Novartis and Amgen, and nonfinancial support from Johnson & Johnson outside the submitted work. No disclosures were reported by the other authors.

Authors' Contributions

C. Falcomatà: Data curation, formal analysis, validation, investigation, visualization, methodology, writing—original draft, writing—review and editing. **S. Bärthel:** Data curation, formal analysis, validation, investigation, visualization, methodology, writing—review and editing. **A. Ulrich:** Formal analysis, investigation, methodology. **S. Diersch:** Investigation, methodology. **C. Veltkamp:** Investigation. **L. Rad:** Conceptualization, formal analysis, supervision, investigation, methodology. **F. Boniolo:** Data curation, software, formal analysis, investigation, visualization. **M. Solar:** Resources, investigation. **K. Steiger:** Formal analysis. **B. Seidler:** Conceptualization, resources, formal analysis, validation, investigation. **M. Zukowska:** Resources, investigation. **J. Madej:** Resources. **M. Wang:** Investigation. **R. Öllinger:** Resources, data curation, formal analysis, investigation. **R. Maresch:** Resources, investigation. **M. Barenboim:** Software, formal analysis. **S. Eser:** Investigation. **M. Tschurtschenthaler:** Investigation. **A. Mehrabi:** Resources. **S. Roessler:** Resources, data curation, formal analysis. **B. Goepfert:** Resources, data curation, investigation. **A. Kind:** Writing—original draft. **A. Schnieke:** Resources, supervision, writing—original draft. **M.S. Robles:** Resources, funding acquisition, validation, investigation. **A. Bradley:** Resources. **R.M. Schmid:** Resources. **M. Schmidt-Supprian:** Resources, funding acquisition, validation, investigation. **M. Reichert:** Resources, investigation. **W. Weichert:** Resources, investigation. **O.J. Sansom:** Resources, data curation, investigation. **J.P. Morton:** Resources, data curation, investigation. **R. Rad:** Resources, software, formal analysis, supervision, validation, investigation, methodology. **G. Schneider:** Conceptualization, resources, supervision, funding acquisition, validation, investigation, writing—review and editing. **D. Saur:** Conceptualization, resources, formal analysis, supervision, funding acquisition, validation, investigation, methodology, writing—original draft, writing—review and editing.

Acknowledgments

We would like to thank Dr. J. Roberts, Dr. T. Jacks, Dr. J. Jonkers, Dr. A. Berns, Dr. A. Lowy, Dr. T. Mak, Dr. L. Luo, Dr. H. Zeng, and

Dr. D. Tuveson for providing transgenic animals and J. Götzfried, M. Mielke, A. Hering, and O. Seelbach for excellent technical assistance. This work was supported by funding from Deutsche Forschungsgemeinschaft (DFG SA 1374/4-3 to D. Saur, SFB 1321 Project-ID 329628492, P06, P11, P13 to M. Reichert, M. Schmidt-Supprian, G. Schneider, and D. Saur, and S1 to W. Weichert and K. Steiger), SFB 1371 Project-ID 395357507 P12 to D. Saur), the German Cancer Consortium (DKTK to K. Steiger, M. Schmidt-Supprian, W. Weichert, R. Rad, G. Schneider, and D. Saur), the European Research Council (ERC CoG No. 648521 to D. Saur), Cancer Research UK (CRUK) core funding to the CRUK Beatson Institute (A17196), and CRUK core funding to O.J. Sansom (A21139).

The publication costs of this article were defrayed in part by the payment of publication fees. Therefore, and solely to indicate this fact, this article is hereby marked “advertisement” in accordance with 18 USC section 1734.

Note

Supplementary data for this article are available at Cancer Discovery Online (<http://cancerdiscovery.aacrjournals.org/>).

Received February 12, 2021; revised May 25, 2021; accepted July 1, 2021; published first July 19, 2021.

REFERENCES

- Banales JM, Marin JGG, Lamarca A, Rodrigues PM, Khan SA, Roberts LR, et al. Cholangiocarcinoma 2020: the next horizon in mechanisms and management. *Nat Rev Gastroenterol Hepatol* 2020;17:557–88.
- Rizvi S, Gores GJ. Pathogenesis, diagnosis, and management of cholangiocarcinoma. *Gastroenterology* 2013;145:1215–29.
- Nakamura H, Arai Y, Totoki Y, Shirota T, Elzawahry A, Kato M, et al. Genomic spectra of biliary tract cancer. *Nat Genet* 2015;47:1003–10.
- Zong Y, Stanger BZ. Molecular mechanisms of bile duct development. *Int J Biochem Cell Biol* 2011;43:257–64.
- Spence JR, Lange AW, Lin S-CJ, Kaestner KH, Lowy AM, Kim I, et al. Sox17 regulates organ lineage segregation of ventral foregut progenitor cells. *Dev Cell* 2009;17:62–74.
- Jemal A, Bray F, Center MM, Ferlay J, Ward E, Forman D. Global cancer statistics. *CA Cancer J Clin* 2011;61:69–90.
- Tyson GL, El-Serag HB. Risk factors for cholangiocarcinoma. *Hepatology* 2011;54:173–84.
- Siegel RL, Miller KD, Jemal A. Cancer statistics, 2020. *CA Cancer J Clin* 2020;70:7–30.
- Tian W, Hu W, Shi X, Liu P, Ma X, Zhao W, et al. Comprehensive genomic profile of cholangiocarcinomas in China. *Oncol Lett* 2020;19:3101–10.
- Lowery MA, Ptashkin R, Jordan E, Berger MF, Zehir A, Capanu M, et al. Comprehensive molecular profiling of intrahepatic and extrahepatic cholangiocarcinomas: potential targets for intervention. *Clin Cancer Res* 2018;24:4154–61.
- Fujimoto A, Furuta M, Shiraishi Y, Gotoh K, Kawakami Y, Arihiro K, et al. Whole-genome mutational landscape of liver cancers displaying biliary phenotype reveals hepatitis impact and molecular diversity. *Nat Commun* 2015;6:6120.
- Razumilava N, Gores GJ. Cholangiocarcinoma. *Lancet* 2014;383:2168–79.
- Goepfert B, Konermann C, Schmidt CR, Bogatyrova O, Geiselhart L, Ernst C, et al. Global alterations of DNA methylation in cholangiocarcinoma target the Wnt signaling pathway. *Hepatology* 2014;59:544–54.
- Rad R, Rad L, Wang W, Strong A, Ponstingl H, Bronner IF, et al. A conditional piggyBac transposition system for genetic screening in mice identifies oncogenic networks in pancreatic cancer. *Nat Genet* 2015;47:47–56.
- Rad R, Rad L, Wang W, Cadinanos J, Vassiliou G, Rice S, et al. PiggyBac transposon mutagenesis: a tool for cancer gene discovery in mice. *Science* 2010;330:1104–7.

16. Hingorani SR, Petricoin EF, Maitra A, Rajapakse V, King C, Jacobetz MA, et al. Preinvasive and invasive ductal pancreatic cancer and its early detection in the mouse. *Cancer Cell* 2003;4:437–50.
17. Madisen L, Zwingman TA, Sunkin SM, Oh SW, Zariwala HA, Gu H, et al. A robust and high-throughput Cre reporting and characterization system for the whole mouse brain. *Nat Neurosci* 2010;13:133–40.
18. Muzumdar MD, Tasic B, Miyamichi K, Li L, Luo L. A global double-fluorescent Cre reporter mouse. *Genesis* 2007;45:593–605.
19. Chong DQ, Zhu AX. The landscape of targeted therapies for cholangiocarcinoma: current status and emerging targets. *Oncotarget* 2016;7:46750–67.
20. Rizvi S, Borad MJ, Patel T, Gores GJ. Cholangiocarcinoma: molecular pathways and therapeutic opportunities. *Semin Liver Dis* 2014;34:456–64.
21. Deshpande V, Nduaguba A, Zimmerman SM, Kehoe SM, Macconail LE, Lauwers GY, et al. Mutational profiling reveals PIK3CA mutations in gallbladder carcinoma. *BMC Cancer* 2011;11:60.
22. Yoo KH, Kim NKD, Kwon WI, Lee C, Kim SY, Jang J, et al. Genomic alterations in biliary tract cancer using targeted sequencing. *Transl Oncol* 2016;9:173–8.
23. Zou S, Li J, Zhou H, Frech C, Jiang X, Chu JSC, et al. Mutational landscape of intrahepatic cholangiocarcinoma. *Nat Commun* 2014;5:5696.
24. Eser S, Reiff N, Messer M, Seidler B, Gottschalk K, Dobler M, et al. Selective requirement of PI3K/PDK1 signaling for Kras oncogene-driven pancreatic cell plasticity and cancer. *Cancer Cell* 2013;23:406–20.
25. Bader AG, Kang S, Zhao L, Vogt PK. Oncogenic PI3K deregulates transcription and translation. *Nat Rev Cancer* 2005;5:921–9.
26. Pylayeva-Gupta Y, Grabocka E, Bar-Sagi D. RAS oncogenes: weaving a tumorigenic web. *Nat Rev Cancer* 2011;11:761–74.
27. Zen Y, Adsay NV, Bardadin K, Colombari R, Ferrell L, Haga H, et al. Biliary intraepithelial neoplasia: an international interobserver agreement study and proposal for diagnostic criteria. *Mod Pathol* 2007;20:701–9.
28. Baer R, Cintas C, Dufresne M, Cassant-Sourdy S, Schönhuber N, Planque L, et al. Pancreatic cell plasticity and cancer initiation induced by oncogenic Kras is completely dependent on wild-type PI 3-kinase p110 α . *Genes Dev* 2014;28:2621–35.
29. Esposito I, Schirmacher P. Pathological aspects of cholangiocarcinoma. *HPB (Oxford)* 2008;10:83–6.
30. O'Dell MR, Huang JL, Whitney-Miller CL, Deshpande V, Rothberg P, Grose V, et al. Kras(G12D) and p53 mutation cause primary intrahepatic cholangiocarcinoma. *Cancer Res* 2012;72:1557–67.
31. Jackson EL, Willis N, Mercer K, Bronson RT, Crowley D, Montoya R, et al. Analysis of lung tumor initiation and progression using conditional expression of oncogenic K-ras. *Genes Dev* 2001;15:3243–8.
32. Morton JP, Timpson P, Karim SA, Ridgway RA, Athineos D, Doyle B, et al. Mutant p53 drives metastasis and overcomes growth arrest/senescence in pancreatic cancer. *Proc Natl Acad Sci U S A* 2010;107:246–51.
33. Caldwell ME, DeNicola GM, Martins CP, Jacobetz MA, Maitra A, Hruban RH, et al. Cellular features of senescence during the evolution of human and murine ductal pancreatic cancer. *Oncogene* 2012;31:1599–608.
34. Schofield HK, Zeller J, Espinoza C, Halbrook CJ, del Vecchio A, Magnuson B, et al. Mutant p53R270H drives altered metabolism and increased invasion in pancreatic ductal adenocarcinoma. *JCI Insight* 2018;3:e97422.
35. Jonkers J, Meuwissen R, van der Gulden H, Peterse H, van der Valk M, Berns A. Synergistic tumor suppressor activity of BRCA2 and p53 in a conditional mouse model for breast cancer. *Nat Genet* 2001;29:418–25.
36. Sarver AL, Erdman J, Starr T, Largaespada DA, Silverstein KAT. TAPDANCE: an automated tool to identify and annotate transposon insertion CISs and associations between CISs from next generation sequence data. *BMC Bioinformatics* 2012;13:154.
37. Lo Re AE, Fernandez-Barrena MG, Almada LL, Mills LD, Elsawa SF, Lund G, et al. Novel AKT1-GLI3-VMP1 pathway mediates KRAS oncogene-induced autophagy in cancer cells. *J Biol Chem* 2012;287:25325–34.
38. Szklarczyk D, Franceschini A, Wyder S, Forslund K, Heller D, Huerta-Cepas J, et al. STRING v10: protein-protein interaction networks, integrated over the tree of life. *Nucleic Acids Res* 2015;43:D447–52.
39. Suzuki A, Yamaguchi MT, Ohteki T, Sasaki T, Kaisho T, Kimura Y, et al. T cell-specific loss of Pten leads to defects in central and peripheral tolerance. *Immunity* 2001;14:523–34.
40. Tumaneng K, Schlegelmilch K, Russell RC, Yimlamai D, Basnet H, Mahadevan N, et al. YAP mediates crosstalk between the Hippo and PI(3)K-TOR pathways by suppressing PTEN via miR-29. *Nat Cell Biol* 2012;14:1322–9.
41. Yim EK, Peng G, Dai H, Hu R, Li K, Lu Y, et al. Rak functions as a tumor suppressor by regulating PTEN protein stability and function. *Cancer Cell* 2009;15:304–14.
42. Chu IM, Hengst L, Slingerland JM. The Cdk inhibitor p27 in human cancer: prognostic potential and relevance to anticancer therapy. *Nat Rev Cancer* 2008;8:253–67.
43. Masuda K, Ishikawa Y, Onoyama I, Unno M, de Alboran IM, Nakayama KI, et al. Complex regulation of cell-cycle inhibitors by Fbxw7 in mouse embryonic fibroblasts. *Oncogene* 2010;29:1798–809.
44. Lee YH, Seo D, Choi KJ, Andersen JB, Won MA, Kitade M, et al. Antitumor effects in hepatocarcinoma of isoform-selective inhibition of HDAC2. *Cancer Res* 2014;74:4752–61.
45. Lin HK, Chen Z, Wang G, Nardella C, Lee SW, Chan CH, et al. Skp2 targeting suppresses tumorigenesis by Arf-p53-independent cellular senescence. *Nature* 2010;464:374–9.
46. Lin HK, Wang G, Chen Z, Teruya-Feldstein J, Liu Y, Chan CH, et al. Phosphorylation-dependent regulation of cytosolic localization and oncogenic function of Skp2 by Akt/PKB. *Nat Cell Biol* 2009;11:420–32.
47. Pearce LR, Komander D, Alessi DR. The nuts and bolts of AGC protein kinases. *Nat Rev Mol Cell Biol* 2010;11:9–22.
48. Fruman DA, Rommel C. PI3K and cancer: lessons, challenges and opportunities. *Nat Rev Drug Discov* 2014;13:140–56.
49. Pang M, Ma L, Liu N, Ponnusamy M, Zhao TC, Yan H, et al. Histone deacetylase 1/2 mediates proliferation of renal interstitial fibroblasts and expression of cell cycle proteins. *J Cell Biochem* 2011;112:2138–48.
50. Yang J, Yuan D, Li J, Zheng S, Wang B. miR-186 downregulates protein phosphatase PPM1B in bladder cancer and mediates G1-S phase transition. *Tumour Biol* 2016;37:4331–41.
51. Churi CR, Shroff R, Wang Y, Rashid A, Kang HC, Weatherly J, et al. Mutation profiling in cholangiocarcinoma: prognostic and therapeutic implications. *PLoS One* 2014;9:e115383.
52. Lee-Hoeflich ST, Pham TQ, Dowbenko D, Munroe X, Lee J, Li L, et al. PPM1H is a p27 phosphatase implicated in trastuzumab resistance. *Cancer Discov* 2011;1:326–37.
53. Jarnagin WR, Klimstra DS, Hezel M, Gonen M, Fong Y, Roggin K, et al. Differential cell cycle-regulatory protein expression in biliary tract adenocarcinoma: correlation with anatomic site, pathologic variables, and clinical outcome. *J Clin Oncol* 2006;24:1152–60.
54. Diersch S, Wenzel P, Szameitat M, Eser P, Paul MC, Seidler B, et al. Efemp1 and p27(Kip1) modulate responsiveness of pancreatic cancer cells towards a dual PI3K/mTOR inhibitor in preclinical models. *Oncotarget* 2013;4:277–88.
55. Kelly-Spratt KS, Philipp-Staheli J, Gurley KE, Hoon-Kim K, Knoblaugh S, Kemp CJ. Inhibition of PI-3K restores nuclear p27Kip1 expression in a mouse model of Kras-driven lung cancer. *Oncogene* 2009;28:3652–62.
56. Fero ML, Rivkin M, Tasch M, Porter P, Carow CE, Firpo E, et al. A syndrome of multiorgan hyperplasia with features of gigantism, tumorigenesis, and female sterility in p27(Kip1)-deficient mice. *Cell* 1996;85:733–44.
57. Fiorentino M, Altamari A, D'Errico A, Gabusi E, Chieco P, Masetti M, et al. Low p27 expression is an independent predictor of survival for patients with either hilar or peripheral intrahepatic cholangiocarcinoma. *Clin Cancer Res* 2001;7:3994–9.

58. Jones RP, Bird NTE, Smith RA, Palmer DH, Fenwick SW, Poston GJ, et al. Prognostic molecular markers in resected extrahepatic biliary tract cancers; a systematic review and meta-analysis of immunohistochemically detected biomarkers. *Biomark Med* 2015;9:763–75.
59. Ruys AT, Groot Koerkamp B, Wiggers JK, Klumpen HJ, ten Kate FJ, van Gulik TM. Prognostic biomarkers in patients with resected cholangiocarcinoma: a systematic review and meta-analysis. *Ann Surg Oncol* 2014;21:487–500.
60. Schneider G, Schmidt-Supprian M, Rad R, Saur D. Tissue-specific tumorigenesis: context matters. *Nat Rev Cancer* 2017;17:239–53.
61. Tuveson D, Hanahan D. Translational medicine: cancer lessons from mice to humans. *Nature* 2011;471:316–7.
62. Jonkers J, Berns A. Conditional mouse models of sporadic cancer. *Nat Rev Cancer* 2002;2:251–65.
63. Eser S, Messer M, Eser P, von Werder A, Seidler B, Bajbouj M, et al. In vivo diagnosis of murine pancreatic intraepithelial neoplasia and early-stage pancreatic cancer by molecular imaging. *Proc Natl Acad Sci U S A* 2011;108:9945–50.
64. Lee H, Wang K, Johnson A, Jones DM, Ali SM, Elvin JA, et al. Comprehensive genomic profiling of extrahepatic cholangiocarcinoma reveals a long tail of therapeutic targets. *J Clin Pathol* 2016;69:403–8.
65. Huang X, Dixit VM. Drugging the undruggables: exploring the ubiquitin system for drug development. *Cell Res* 2016;26:484–98.
66. Hruban RH, Adsay NV, Albores-Saavedra J, Anver MR, Biankin AV, Boivin GP, et al. Pathology of genetically engineered mouse models of pancreatic exocrine cancer: consensus report and recommendations. *Cancer Res* 2006;66:95–106.
67. Albores-Saavedra J, Henson DE, Klimstra DS. Tumors of the gallbladder, extrahepatic bile ducts, and Vaterian system. Silver Spring (MD) American Registry of Pathology; 2015.
68. von Burstin J, Eser S, Paul MC, Seidler B, Brandl M, Messer M, et al. E-cadherin regulates metastasis of pancreatic cancer in vivo and is suppressed by a SNAIL/HDAC1/HDAC2 repressor complex. *Gastroenterology* 2009;137:361–71.
69. Mueller S, Engleitner T, Maresch R, Zukowska M, Lange S, Kaltenbacher T, et al. Evolutionary routes and KRAS dosage define pancreatic cancer phenotypes. *Nature* 2018;554:62–8.
70. Glass K, Huttenhower C, Quackenbush J, Yuan GC. Passing messages between biological networks to refine predicted interactions. *PLoS One* 2013;8:e64832.